Coupled Systems Mechanics, *Vol. 14, No. 1 (2025) 57-86*
https://doi.org/10.12989/csm.2025.14.1.057

Application of mixed high order-Wavenumber approach in dynamic analysis of Pine Flat dam-reservoir system

Vahid Lotfi* and Solmaz Dehghanmarvasty[a]

Department of Civil and Environmental Engineering, Amirkabir University of Technology, Tehran, Iran

(Received June 11, 2024, Revised February 7, 2025, Accepted March 23, 2025)

Abstract. Recently, mixed HO-WN (i.e., High order-Wavenumber) method was introduced for dynamic analysis of concrete gravity dam-reservoir systems. This is formulated by FE-(FE-TE) approach (i.e., Finite Element-(Finite Element-Truncation Element)). In this technique, dam and reservoir are discretized by plane solid and fluid finite elements. Moreover, the mixed HO-WN (i.e., High order-Wavenumber) condition imposed at the reservoir truncation boundary. This task is formulated by employing a truncation element at that boundary. It should be emphasized that three alternatives are discussed for this approach. The first two alternatives result in one additional degree of freedom at each node in comparison with usual modeling in practice which employs Sommerfeld truncation condition. While, the third alternative leads to two additional degrees of freedom. The method in each case is generally derived by combining the High-order and Wavenumber approaches. The formulation is initially reviewed which was originally proposed in a previous study. Thereafter, the response of Pine Flat dam-reservoir system is studied due to horizontal and vertical ground motions for two types of reservoir bottom conditions of full reflective and absorptive. The initial part of study is focused on the time harmonic analysis. In this part, it is possible to compare the transfer functions against corresponding responses obtained by FE-(FE-HE) (i.e., Finite Element-(Finite Element-Hyper Element)) approach (referred to as exact method). Subsequently, the transient analysis is carried out. In that part, the results in each case are compared against the corresponding results obtained by the high order H-W (i.e., Hagstrom-Warburton) condition applied on the truncation boundary. It is worthwhile to emphasize that results for high order H-W condition (e.g., O5-5) are not sensitive to L/H (i.e., normalized reservoir length) value. Therefore, they can be envisaged as exact results (in numerical sense) in time domain.

Keywords: absorbing boundary conditions; concrete gravity dams; high-order condition; truncation boundary; Wavenumber approach

1. Introduction

Fluid-structure interaction has captured the interest of many researchers (Hadzalic *et al*. 2018, 2019, Lotfi and Sharghi 2000, 2001, Hosseinzadeh *et al*. 2013, Arjmandi and Lotfi 2011, 2013, Sani and Lotfi 2007, 2011). Moreover, there has been extensive research about dynamic analysis of concrete gravity dam-reservoir systems in particular. This was mainly carried out by the

*Corresponding author, Professor, E-mail: vahlotfi@aut.ac.ir
[a]Ph.D. Candidate

http://www.techno-press.org/?journal=csm&subpage=8 ISSN: 2234-2184 (Print), 2234-2192 (Online)

rigorous FE-(FE-HE) (i.e., Finite Element-(Finite Element-Hyper Element)) method in the frequency domain. This means that the dam is discretized by plane solid finite elements, while, the reservoir is divided into two parts, a near-field region (usually an irregular shape) in the vicinity of the dam and a far-field part (assuming constant depth) which extends to infinity in the upstream direction. The former region is discretized by fluid finite elements and the latter part is modeled by a two-dimensional fluid hyper-element (Hall and Chopra 1982, Waas 1972). It is also understood that employing fluid hyper-element would lead to the exact solution (in numerical sense) of the problem. However, it is formulated in the frequency domain and its application in this field has led to many especial purpose programs which were demanding from programming point of view.

On the other hand, engineers have often tried to solve this problem in the context of pure finite element programming (FE-FE method of analysis). In this approach, an often simplified condition is imposed on the truncation boundary or the upstream face of the near-field water domain. Thus, the fluid hyper-element is actually excluded from the model. One of these widely used methods is based on Sommerfeld truncation boundary condition (Sommerfeld 1949). The main advantage of this condition is that it can be readily used for time domain analysis. Thus, they are also vastly employed in nonlinear seismic analysis of concrete dams (Lokke and Chopra 2017, Lokke and Chopra 2018). However, its major shortcoming is that the results have significant errors when low normalized reservoir lengths are utilized (Lotfi and Zenz 2016, Lotfi and Zenz 2018, Farzad and Lotfi 2023). Moreover, there are also many studies which have employed Westergaard approach for seismic analysis of concrete dams to simplify dam-reservoir interaction even further (Karabulut and Kartal 2018, Lotfi and Omidi 2012, Akbari and Lotfi 2022, Akbari *et al*. 2023).

Of course, there have also been many researches in the last three decades to develop more accurate absorbing boundary conditions to be applied for similar fluid-structure or soil-structure interaction problems. It should be emphasized that many of these studies are actually limited their works to two-dimensional cases. Perfectly matched layer (Berenger 1994, Chew and Weedon 1994, Basu and Chopra 2003, Jiong *et al*. 2009, Kim and Pasciak 2012, Khazaee and Lotfi 2014a, Khazaee and Lotfi 2014b) and, high-order non-reflecting boundary condition (Higdon 1986, Givoli and Neta 2003, Hagstrom and Warburton 2004, Givoli, *et al.* 2006, Hagstrom *et al.* 2008, Rabinovich *et al.* 2011, Samii and Lotfi 2012, Lotfi and Lotfi 2021, 2022, Dehghanmarvasty and Lotfi 2023) are among the two main popular groups of methods which researchers have applied in their attempts. It is emphasized that these techniques have become very popular in recent years due to the fact that they could be applied in time domain as well as the frequency domain.

Furthermore, the Wavenumber approach was introduced in 2012 based on the FE method. Initially, this approach was introduced just for horizontal ground excitation and full reflective reservoir base condition (Lotfi and Samii 2012). Later on, some modifications were implemented to expand the technique for general reservoir base condition (Jafari and Lotfi 2018). Subsequently, it was discussed for the general reservoir base condition and ground excitation (Lotfi 2017). Of course, it is worthwhile to emphasize that these initial studies were developed for frequency domain analysis. However, it was also later expanded for transient analysis (Ganji and Lotfi 2021, Lotfi and Zenz 2022).

More recently, a new method is introduced for dynamic analysis of concrete gravity dam-reservoir systems which is referred to as mixed High order-Wavenumber (HO-WN) approach (Lotfi and Dehghanmarvasty 2023). This is based on FE-(FE-TE) (i.e., Finite Element-(Finite Element-Truncation Element)) procedure. The core of the method is based on utilizing a truncation-element at the U/S (i.e., Upstream) truncation boundary of the reservoir near-field domain and excluding far-field region of the reservoir. This truncation-element is formulated

based on the mixed High order-Wavenumber (HO-WN) condition applied at that boundary. The method is derived by combining the High-order and Wavenumber approaches.

The present study is focused on applying mixed High order-Wavenumber (HO-WN) approach for dynamic analysis of concrete gravity dam-reservoir systems. The formulation is initially reviewed which was originally proposed in a previous study (Lotfi and Dehghanmarvasty 2023). It should be emphasized that three alternatives are discussed for this approach. The first two alternatives result in one additional degree of freedom at each node in comparison with usual modeling in practice which employs Sommerfeld truncation condition. While, the third alternative leads to two additional degrees of freedom. In this respect, a special purpose finite element program (Lotfi 2001a) is enhanced for this investigation. Thereafter, the response of Pine Flat dam-reservoir system is studied due to horizontal and vertical ground motions. Furthermore, two conditions of full reflective and absorptive reservoir bottom are considered.

The initial part of study is focused on the time harmonic analysis. In this part, it is possible to compare the transfer functions against corresponding responses obtained by rigorous FE-(FE-HE) approach (referred to as exact method). Subsequently, the transient analysis is carried out. In that part, the results in each case are compared against the corresponding results obtained by the high order H-W condition applied on the truncation boundary. It is worthwhile to emphasize that results for high order H-W condition (e.g., O5-5) are not sensitive to *L/H* value. Therefore, they can be envisaged as exact results (in numerical sense) in time domain.

It is also worthwhile to emphasize that simplified Sommerfeld condition does not produce accurate results for low values of normalized reservoir length as previously mentioned. This is due to the fact that Sommerfeld condition is merely designed for incident-wave propagating normal to the truncation boundary and it is not appropriate for inclined incident waves (Lotfi and Zenz 2016, Lotfi and Zenz 2018). Therefore, one would prefer more advanced conditions as decided in the present study.

2. Method of analysis

As mentioned, the analysis technique utilized in this study is based on the FE-(FE-TE) method, which is applicable for a general concrete gravity dam-reservoir system. The formulation is described in great details in the previous study (Lotfi and Dehghanmarvasty 2023). However, the salient aspects of the approach will be reviewed in this section.

For this aim, let us consider a concrete gravity dam-reservoir system. The coupled equations can be obtained by considering each region separately and then combine the resulting equations.

2.1 Dam body

Concentrating on the structural part, the dynamic behavior of the dam is described by the well-known equation of structural dynamics (Zienkiewicz and Taylor 2000)

$$\mathbf{M}\,\ddot{\mathbf{r}} + \mathbf{C}\,\dot{\mathbf{r}} + \mathbf{K}\,\mathbf{r} = -\widetilde{\mathbf{M}}\,\mathbf{J}\,\mathbf{a}_{\mathrm{g}} + \mathbf{B}^{\mathrm{T}}\mathbf{P} \tag{1}$$

where **M**, **C** and **K** in this relation represent mass, damping and stiffness matrices of the dam body. Moreover, **r** is the vector of nodal relative displacements, $\widetilde{\mathbf{M}}$ is the same as **M** matrix except that no columns are excluded due to restraints, **J** is a matrix with each two rows equal to a 2×2 identity matrix (its columns correspond to a unit horizontal and vertical rigid body motion) and $\mathbf{a}_{\mathrm{g}}$ denotes

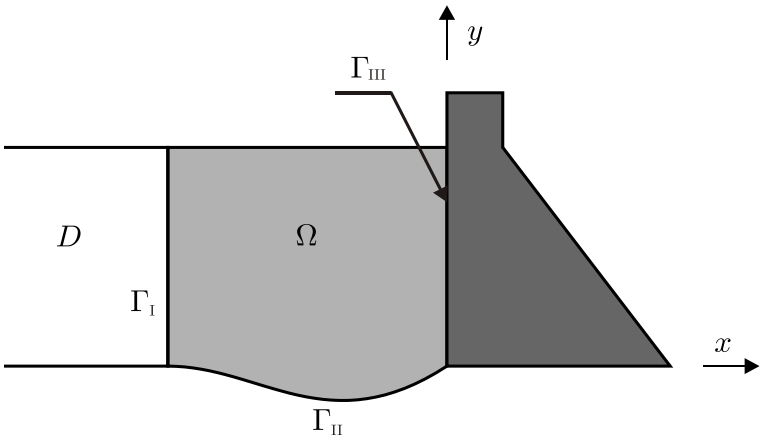

Fig. 1 Schematic view of a typical dam-reservoir system. The near-field reservoir domain **Ω**, the truncation boundary Γ_I and the far-field region *D*

the vector of ground accelerations in two directions. Furthermore, **B** is a matrix which relates vectors of hydrodynamic pressures (i.e., **P**), and its equivalent nodal forces.

2.2 Water domain

Assuming water to be linearly compressible and neglecting its viscosity, its small irrotational motion (Fig. 1) is governed by the wave equation (Chopra 1967, Chopra, *et al.* 1980)

$$\nabla^2 P - \frac{1}{c^2}\ddot{P} = 0 \ ; \qquad \text{in } \Omega \text{ and D} \tag{2}$$

where *P* is the hydrodynamic pressure and, *c* is the pressure wave velocity in water. Apart from truncation boundary condition for upstream face of the water domain (Γ_I) which is discussed on subsequent sections, the boundary conditions for water domain are as follows

$$\partial_n P = -\rho a_g^n - q\dot{P} \ ; \quad \text{at reservoir's bottom } (\Gamma_{II}) \tag{3a}$$

$$\partial_n P = -\rho\, \ddot{u}_n \ ; \quad \text{at dam-water interface } (\Gamma_{III}) \tag{3b}$$

$$P = 0 \ ; \qquad \text{on water surface } (\Gamma_{IV}) \tag{3c}$$

Herein, ρ is the water density and *n* denotes the outward perpendicular direction (with respect to fluid region) and $\ddot{u}_n$ is the normal acceleration of fluid particles at dam-reservoir interface which is equal to solid particle total acceleration in that direction due to compatibility of acceleration. It should be also emphasized that $\partial_n P$ refers to partial derivative of *P* with respect to *n*-direction (i.e., $\partial_n P = \partial P/\partial n$). Moreover, the admittance or damping coefficient q utilized in Eq. (3a), may be related to a more meaningful wave reflection coefficient α (Fenves and Chopra 1985)

$$\alpha = \frac{1 - qc}{1 + qc} \tag{4}$$

which is defined as the ratio of the amplitude of reflected hydrodynamic pressure wave to the

amplitude of incident pressure wave normal to the reservoir's bottom. For a fully reflective reservoir's bottom condition, α is equal to 1 which leads to $q = 0$.

One can apply the weighted residual approach to obtain the finite element equation of the fluid domain, which may be written as

$$\mathbf{G}\,\ddot{\mathbf{P}} + q\,\mathbf{L}_{\mathrm{II}}\dot{\mathbf{P}} + \mathbf{H}\,\mathbf{P} = \mathbf{R}_{\mathrm{I}} - \mathbf{B}\,\ddot{\mathbf{r}} - \widetilde{\mathbf{B}}\,\mathbf{J}\,\mathbf{a}_{\mathrm{g}} \tag{5}$$

In this relation, **G**, **H** are fluid domain's generalized mass and stiffness matrices and **P** is the vector of nodal pressures. It should be emphasized that all boundary conditions are already considered in Eq. (5). In particular, the ones related to reservoir bottom's surface (i.e., Γ_{II}; (Fig. 1)) through $\mathbf{L}_{\mathrm{II}}$ matrix, water surface, and the contribution related to the truncation boundary condition is symbolically denoted by the vector $\mathbf{R}_{\mathrm{I}}$. Furthermore, matrix **B**, is resulted due to dam-reservoir boundary condition (i.e., Γ_{III}), which also appears in Eq. (1). Matrix $\widetilde{\mathbf{B}}$ is the same as matrix **B** except that no columns are excluded due to restraints, and it has contributions due to reservoir bottom, as well as dam-reservoir's interface.

It is also worthwhile to emphasize that $\mathbf{R}_{\mathrm{I}}$ is obtained by assembling the following boundary integrals of the fluid elements adjacent to that surface (i.e., Γ_{I})

$$\mathbf{R}^{e} = \frac{1}{\rho}\int_{\Gamma^{e}} \mathbf{N}\,(\partial_n P)\,d\Gamma^{e} \tag{6}$$

With **N** being the vector of element's shape functions and n denotes the fluid element's outward normal direction. It should be emphasized that one may utilize Eq. (6) to obtain $\mathbf{R}_{\mathrm{I}}^{\mathbf{e}}$, if there is merely horizontal excitation. However, the following equation must be employed in general condition that vertical excitation may also exist

$$\mathbf{R}_{\mathbf{I}}^{\mathbf{e}} = \frac{1}{\rho}\int_{\Gamma_I^{e}} \mathbf{N}\,(\partial_n P^{s})\,d\Gamma^{e} \tag{7}$$

It should be stressed that $\partial_n P^s$ refers to partial derivative of P^s with respect to n-direction (i.e, $\partial_n P^s = \partial P^s/\partial n$). Moreover, it is noted that P^s (scattered pressure) term is substituted for P (total pressure), and they are related as follows

$$P^{s} = P - P^{i} \tag{8}$$

The P^i is the incidence pressure contribution which is due to ground acceleration imposed at bottom of uniform part extending to infinity in the upstream direction (Fig. 1). It is noted that this is actually eliminated in our current discretization since it is beyond the truncation boundary. However, incidence pressure's effect is included in the present approach through relations (7) and (8).

Let us now substitute P^s by another function ϕ_0 which is utilized in writing the high-order boundary condition later on

$$\phi_0 = P^{s} \tag{9}$$

Employing this function, relation (7) may be rewritten as follows

$$\mathbf{R}_{\mathbf{I}}^{\mathbf{e}} = \frac{1}{\rho}\int_{\Gamma_I^{e}} \mathbf{N}\,(-\partial_x \phi_0)\,d\Gamma^{e} \tag{10}$$

It is noted that negative sign in this relation is due to the fact that the outward normal is

opposite to the *x*-direction for fluid finite elements adjacent to the truncation boundary (Fig. 1). It is obvious that simplified relations (e.g., Sommerfeld condition) may be utilized in relation (10) to explicitly define that vector. However, that would not produce accurate results for low values of normalized reservoir length as previously mentioned. This is due to the fact that Sommerfeld condition is merely designed for incident-wave propagating normal to the truncation boundary and it is not appropriate for inclined incident waves. Therefore, one would prefer to resort to high-order conditions as presented in Section 3.

2.3 Dam-reservoir system

The necessary equations for both dam and reservoir domains were explained in previous sections. Thus, combining the main relations (1) and (5) would result in the FE equations of the coupled dam-reservoir system in its initial form for the time domain

$$\begin{pmatrix}\mathbf{M} & \mathbf{0}\\ \mathbf{B} & \mathbf{G}\end{pmatrix}\begin{pmatrix}\ddot{\mathbf{r}}\\ \ddot{\mathbf{P}}\end{pmatrix}+\begin{pmatrix}\mathbf{C} & \mathbf{0}\\ \mathbf{0} & q\mathbf{L}_{\mathrm{II}}\end{pmatrix}\begin{pmatrix}\dot{\mathbf{r}}\\ \dot{\mathbf{P}}\end{pmatrix}+\begin{pmatrix}\mathbf{K} & -\mathbf{B}^{\mathrm{T}}\\ \mathbf{0} & \mathbf{H}\end{pmatrix}\begin{pmatrix}\mathbf{r}\\ \mathbf{P}\end{pmatrix}+\begin{pmatrix}\mathbf{0}\\ -\mathbf{R}_{\mathrm{I}}\end{pmatrix}=\begin{pmatrix}-\widetilde{\mathbf{M}}\,\mathbf{J}\,a_{\mathrm{g}}\\ -\widetilde{\mathbf{B}}\,\mathbf{J}\,a_{\mathrm{g}}\end{pmatrix} \tag{11}$$

It is noted from the above equation that vector $\mathbf{R}_{\mathrm{I}}$ still needs to be defined by some appropriate condition. This is related to the truncated boundary Γ_{I}. It is interesting to note that one may presume that there exists a truncation-element attached at this boundary similar to hyper-element role in FE-(FE-HE) approach. The purpose of this element is to generate the vector $\mathbf{R}_{\mathrm{I}}$ based on mixed HO-WN truncation boundary condition. The element will have generalized mass, damping and stiffness matrices similar to usual solid or fluid finite elements. The details will be discussed below.

3. Mixed HO-WN truncation-element

3.1 Basic relations

As mentioned, high-order conditions are the basis of mixed HO-WN truncation boundary. In particular, G-N condition is employed in the present study (Givoli and Neta 2003). However, certain basic relations are obtained which makes the method much more efficient in comparison with the initial G-N high-order condition. In other words, the aim is to decrease the degrees of freedom in comparison with the usual G-N high-order condition (Givoli and Neta 2003). This is carried out by modifying the method with certain relations from wavenumber method explained elsewhere in details (Lotfi and Dehghanmarvasty 2023). For this reason, this is referred to as the mixed HO-WN (i.e., High order-Wavenumber) approach.

For this purpose, three alternatives are considered for our mixed HO-WN condition which its G-N type high-order truncation condition counterparts are illustrated in Table 1 below.

Let us now concentrate on Alt.3 which is the most challenging case among these three alternatives and present the required basic relations for this approach. It is noticed that three propagating and two evanescent terms are considered in this alternative. This will require six degrees of freedom for each node of the truncation element (four additional degrees of freedom in comparison with Sommerfeld type condition) if the usual G-N type high-order procedure is going to be utilized. However, this is reduced in the mixed HO-WN procedure as described below.

As mentioned in Table 1, the initial high-order condition for Alt. 3 is as follows

Table 1 Three different alternatives considered for mixed HO-WN approach

Alternative	G-N type high-order condition counterpart
1	$(\partial_x-\beta)(\partial_x-\bar{c}\partial_t)(\partial_x-\bar{c}\partial_t)\phi_0=0$
2	$(\partial_x-\beta)(\partial_x-\beta)(\partial_x-\bar{c}\partial_t)\phi_0=0$
3	$(\partial_x-\beta)(\partial_x-\beta)(\partial_x-\bar{c}\partial_t)(\partial_x-\bar{c}\partial_t)(\partial_x-\bar{c}\partial_t)\phi_0=0$

$$(\partial_x-\beta)(\partial_x-\beta)(\partial_x-\bar{c}\partial_t)(\partial_x-\bar{c}\partial_t)(\partial_x-\bar{c}\partial_t)\phi_0=0 \tag{12}$$

The basic relations derived in this alternative are given as follows (Lotfi and Dehghanmarvasty 2023)

$$2\bar{c}\left(\tilde{\lambda}_1^2\right)^R\mathbf{L}_\mathrm{I}\left(\dot{\mathbf{P}}-\dot{\mathbf{P}}^i\right)-\tfrac{2\bar{c}}{\widetilde{\omega}}\left(\tilde{\lambda}_1^2\right)^I\mathbf{L}_\mathrm{I}\left(\ddot{\mathbf{P}}-\ddot{\mathbf{P}}^i\right)+\left(\tilde{\lambda}_1^2\right)^R\mathbf{L}_\mathrm{I}\boldsymbol{\Phi}_1+\tfrac{1}{\widetilde{\omega}}\left(\tilde{\lambda}_1^2\right)^I\mathbf{L}_\mathrm{I}\dot{\boldsymbol{\Phi}}_1-\mathbf{L}_\mathrm{I}\boldsymbol{\Phi}_3+4\bar{c}^2\mathbf{L}_\mathrm{I}\ddot{\boldsymbol{\Phi}}_1=\mathbf{0} \tag{13}$$

$$-2\beta\left(\tilde{\lambda}_1^4\right)^R\mathbf{L}_\mathrm{I}\left(\mathbf{P}-\mathbf{P}^i\right)-\tfrac{2\beta}{\widetilde{\omega}}\left(\tilde{\lambda}_1^4\right)^I\mathbf{L}_\mathrm{I}\left(\dot{\mathbf{P}}-\dot{\mathbf{P}}^i\right)+\left(\left(\tilde{\lambda}_1^2\right)^R+\beta^2\right)\mathbf{L}_\mathrm{I}\boldsymbol{\Phi}_3+\tfrac{1}{\widetilde{\omega}}\left(\tilde{\lambda}_1^2\right)^I\mathbf{L}_\mathrm{I}\dot{\boldsymbol{\Phi}}_3+4\beta\bar{c}\left(\tilde{\lambda}_1^2\right)^R\mathbf{L}_\mathrm{I}\dot{\boldsymbol{\Phi}}_1+\frac{4\beta\bar{c}}{\widetilde{\omega}}\left(\tilde{\lambda}_1^2\right)^I\mathbf{L}_\mathrm{I}\ddot{\boldsymbol{\Phi}}_1+2\beta\bar{c}\,\mathbf{L}_\mathrm{I}\dot{\boldsymbol{\Phi}}_3+\bar{c}^2\mathbf{L}_\mathrm{I}\ddot{\boldsymbol{\Phi}}_3=\mathbf{0} \tag{14}$$

Herein, $\mathbf{P}$, $\mathbf{P}^i$, $\boldsymbol{\Phi}_1$, $\boldsymbol{\Phi}_3$ refer to truncation element sub-vectors which include total pressure, incidence pressure and ϕ_1, ϕ_3 degrees of freedom. The superscripts *R* and *I* stands for real and imaginary part of the complex value, respectively. It should be also mentioned that the following matrix definition is also employed at element level to define $\mathbf{L}_\mathrm{I}$ matrix utilized in these equations

$$\mathbf{L}_\mathrm{I}^e=\frac{1}{\rho}\int_{\Gamma_\mathrm{I}^e}\mathbf{N}\,\mathbf{N}^T d\Gamma^e \tag{15}$$

Moreover, $\widetilde{\omega}$ is the dam-reservoir fundamental frequency. It is also worthwhile to mention that in general λ_1 can be defined through the following Eigenvalue problem

$$cos\left(\lambda_j\mathrm{H}\right)+\frac{i\omega q}{\lambda_j}sin\left(\lambda_j\mathrm{H}\right)=0 \tag{16}$$

It should be noted that λ_1 is constant (i.e., $\lambda_1=\pi/(2H)$, H is the water depth) for full reflective reservoir bottom condition while it is frequency dependent in general condition. In this respect, $\tilde{\lambda}_1$ is denoted as the first Eigenvalue of the above problem corresponding to fundamental frequency of dam-reservoir system.

Apart from the initial basic relations (i.e., Eqs. (13) and (14)), one can also obtain an additional basic relation (on the basis of Eq. (10)) for the mixed HO-WN truncation element as follows (Lotfi and Dehghanmarvasty 2023)

$$\mathbf{L}_\mathrm{I}\boldsymbol{\Phi}_1+\bar{c}\,\mathbf{L}_\mathrm{I}\left(\dot{\mathbf{P}}-\dot{\mathbf{P}}^i\right)+\mathbf{R}_\mathrm{I}^e=\mathbf{0} \tag{17}$$

With the following definition being employed

$$\bar{c}=\frac{1}{c} \tag{18}$$

Furthermore, a complementary relation is required to define incidence pressure wave vector which is written as follows (Lotfi and Dehghanmarvasty 2023)

Table 2 Explicit form of generalized matrix $\mathbf{M}_{\mathrm{I}}$ (Alt.3)

	$\mathbf{P}^{\mathrm{T}}$	$\mathbf{\Phi}_1^{\mathrm{T}}$	$\mathbf{\Phi}_3^{\mathrm{T}}$	$\mathbf{P}^{i\mathrm{T}}$
$\mathbf{P}$	$\mathbf{0}$	$\mathbf{0}$	$\mathbf{0}$	$\mathbf{0}$
$\mathbf{\Phi}_1$	$-\frac{2\bar{c}}{\tilde{\omega}}\left(\tilde{\lambda}_1^2\right)^I\mathbf{L}_{\mathrm{I}}$	$4\bar{\mathrm{c}}^2\mathbf{L}_{\mathrm{I}}$	$\mathbf{0}$	$\frac{2\bar{c}}{\tilde{\omega}}\left(\tilde{\lambda}_1^2\right)^I\mathbf{L}_{\mathrm{I}}$
$\mathbf{\Phi}_3$	$\mathbf{0}$	$\frac{4\beta\bar{c}}{\tilde{\omega}}\left(\tilde{\lambda}_1^2\right)^I\mathbf{L}_{\mathrm{I}}$	$\bar{\mathrm{c}}^2\mathbf{L}_{\mathrm{I}}$	$\mathbf{0}$
$\mathbf{P}^i$	$\mathbf{0}$	$\mathbf{0}$	$\mathbf{0}$	$\bar{\mathrm{c}}^2\mathbf{L}_{\mathrm{I}}$

Table 3 Explicit form of generalized matrix $\mathbf{C}_{\mathrm{I}}$ (Alt.3)

	$\mathbf{P}^{\mathrm{T}}$	$\mathbf{\Phi}_1^{\mathrm{T}}$	$\mathbf{\Phi}_3^{\mathrm{T}}$	$\mathbf{P}^{i\mathrm{T}}$
$\mathbf{P}$	$\bar{\mathrm{c}}\,\mathbf{L}_{\mathrm{I}}$	$\mathbf{0}$	$\mathbf{0}$	$-\bar{\mathrm{c}}\,\mathbf{L}_{\mathrm{I}}$
$\mathbf{\Phi}_1$	$-2\bar{c}\left(\tilde{\lambda}_1^2\right)^R\mathbf{L}_{\mathrm{I}}$	$\frac{1}{\tilde{\omega}}\left(\tilde{\lambda}_1^2\right)^I\mathbf{L}_{\mathrm{I}}$	$\mathbf{0}$	$2\bar{c}\left(\tilde{\lambda}_1^2\right)^R\mathbf{L}_{\mathrm{I}}$
$\mathbf{\Phi}_3$	$-\frac{2\beta}{\tilde{\omega}}\left(\tilde{\lambda}_1^4\right)^I\mathbf{L}_{\mathrm{I}}$	$+4\beta\bar{c}\left(\tilde{\lambda}_1^2\right)^R\mathbf{L}_{\mathrm{I}}$	$\left(\frac{1}{\tilde{\omega}}\left(\tilde{\lambda}_1^2\right)^I+2\beta\bar{c}\right)\mathbf{L}_{\mathrm{I}}$	$\frac{2\beta}{\tilde{\omega}}\left(\tilde{\lambda}_1^4\right)^I\mathbf{L}_{\mathrm{I}}$
$\mathbf{P}^i$	$\mathbf{0}$	$\mathbf{0}$	$\mathbf{0}$	Q_{I}

$$\bar{c}^2\,\mathbf{L}_{\mathrm{I}}\,\ddot{\mathbf{P}}^i+\mathbf{D}_{\mathrm{I}}\,\mathbf{P}^i+\left[\frac{1}{\rho}\left(q\,\dot{P}^i-\rho a_g^y\right)\Big|_{y=0}\right]\tilde{\mathbf{I}}_{\mathrm{I}}=\mathbf{0} \tag{19}$$

With the underneath definition being utilized

$$\tilde{\mathbf{I}}_{\mathrm{I}}=[1\quad 0\quad \ldots\ldots\quad 0\quad 0]^{\mathrm{T}} \tag{20}$$

It can also be written as

$$\bar{c}^2\,\mathbf{L}_{\mathrm{I}}\,\ddot{\mathbf{P}}^i+\mathbf{Q}_{\mathrm{I}}\,\dot{\mathbf{P}}^i+\mathbf{D}_{\mathrm{I}}\,\mathbf{P}^i=-\mathbf{E}_{\mathrm{I}}^i\,\mathbf{a}_g \tag{21}$$

By employing the following matrix definitions

$$\mathbf{Q}_{\mathrm{I}}=\frac{q}{\rho}\tilde{\mathbf{I}}_{\mathrm{I}}\,\tilde{\mathbf{I}}_{\mathrm{I}}{}^{\mathrm{T}} \tag{22}$$

$$\mathbf{E}_{\mathrm{I}}^i=[\mathbf{0}\quad -\tilde{\mathbf{I}}_{\mathrm{I}}] \tag{23}$$

3.2 Generalized matrices of mixed HO-WN truncation-element

Relation (21) was the last required matrix relation for applying mixed HO-WN truncation-element. Therefore, a complete equation set is obtained which is comprised of relations (17), (13), (14), and (21). These relations are now written in the following compacted form

$$\mathbf{M}_{\mathrm{I}}\ddot{\mathbf{P}}_{\mathrm{I}}+\mathbf{C}_{\mathrm{I}}\dot{\mathbf{P}}_{\mathrm{I}}+\mathbf{K}_{\mathrm{I}}\mathbf{P}_{\mathrm{I}}+\widetilde{\mathbf{R}}_{\mathrm{I}}=\mathbf{F}_{\mathrm{I}} \tag{24}$$

It is worthwhile to define the following vectors employed in Eq. (24)

$$\mathbf{P}_{\mathrm{I}}=\left(\mathbf{P}^{\mathrm{T}}\quad \mathbf{\Phi}_1^{\mathrm{T}}\quad \mathbf{\Phi}_3^{\mathrm{T}}\quad \mathbf{P}^{i\mathrm{T}}\right)^{\mathrm{T}} \tag{25}$$

$$\widetilde{\mathbf{R}}_{\mathrm{I}}=(\mathbf{R}_{\mathrm{I}}^{\mathrm{T}}\quad \mathbf{0}\quad \mathbf{0}\quad \mathbf{0})^{\mathrm{T}} \tag{26}$$

$$\mathbf{F}_{\mathrm{I}}=\left(\mathbf{0}\quad \mathbf{0}\quad \mathbf{0}\quad (-\mathbf{E}_{\mathrm{I}}^i\,\mathbf{a}_g)^{\mathrm{T}}\right)^{\mathrm{T}} \tag{27}$$

Table 4 Explicit form of generalized matrix $\mathbf{K}_{\mathrm{I}}$ (Alt.3)

	$\mathbf{P}^{\mathrm{T}}$	$\boldsymbol{\Phi}_1^{\mathrm{T}}$	$\boldsymbol{\Phi}_3^{\mathrm{T}}$	$\mathbf{P}^{i\mathrm{T}}$
$\mathbf{P}$	$\mathbf{0}$	$\mathbf{L}_{\mathrm{I}}$	$\mathbf{0}$	$\mathbf{0}$
$\boldsymbol{\Phi}_1$	$\mathbf{0}$	$\left(\tilde{\lambda}_1^2\right)^R\mathbf{L}_{\mathrm{I}}$	$-\mathbf{L}_{\mathrm{I}}$	$\mathbf{0}$
$\boldsymbol{\Phi}_3$	$-2\beta\left(\tilde{\lambda}_1^4\right)^R\mathbf{L}_{\mathrm{I}}$	0	$\left(\left(\tilde{\lambda}_1^2\right)^R+\beta^2\right)\mathbf{L}_{\mathrm{I}}$	$2\beta\left(\tilde{\lambda}_1^4\right)^R\mathbf{L}_{\mathrm{I}}$
$\mathbf{P}^i$	$\mathbf{0}$	$\mathbf{0}$	$\mathbf{0}$	$\mathbf{D}_{\mathrm{I}}$

Moreover, details of generalized matrices (i.e., $\mathbf{M}_{\mathrm{I}}, \mathbf{C}_{\mathrm{I}}, \mathbf{K}_{\mathrm{I}}$) are provided in Tables 2-4 above:

It is worthwhile to mention that similar matrices are provided for Alt.1 and Alt.2 version of mixed HO-WN approach in Appendices A and B, respectively.

4. Coupled equations of dam-reservoir system

The matrix equation of dam-reservoir system was already presented in sub-section 2.3 (i.e., Eq. (11)). Combining that equation with relation (24) would result in the coupled equation of dam-reservoir system in its final form

$$\begin{pmatrix}\mathbf{M} & \mathbf{0}\\ \bar{\mathbf{B}} & \bar{\mathbf{G}}+\bar{\mathbf{M}}_{\mathrm{I}}\end{pmatrix}\begin{pmatrix}\ddot{\mathbf{r}}\\ \ddot{\bar{\mathbf{P}}}\end{pmatrix}+\begin{pmatrix}\mathbf{C} & \mathbf{0}\\ \mathbf{0} & q\bar{\mathbf{L}}_{\mathrm{II}}+\bar{\mathbf{C}}_{\mathrm{I}}\end{pmatrix}\begin{pmatrix}\dot{\mathbf{r}}\\ \dot{\bar{\mathbf{P}}}\end{pmatrix}+\begin{pmatrix}\mathbf{K} & -\bar{\mathbf{B}}^{\mathrm{T}}\\ \mathbf{0} & \bar{\mathbf{H}}+\bar{\mathbf{K}}_{\mathrm{I}}\end{pmatrix}\begin{pmatrix}\mathbf{r}\\ \bar{\mathbf{P}}\end{pmatrix}=\begin{pmatrix}-\widetilde{\mathbf{M}}\,\mathbf{J}\,\mathbf{a}_{\mathrm{g}}\\ -\bar{\bar{\mathbf{B}}}\,\mathbf{J}\,\mathbf{a}_{\mathrm{g}}+\bar{\mathbf{F}}_{\mathrm{I}}\end{pmatrix} \tag{28}$$

It is noted that vectors $\widetilde{\mathbf{R}}_{\mathrm{I}}$ and $-\mathbf{R}_{\mathrm{I}}$ cancel each other during this process. Furthermore, the bar sign over matrices emphasize that they are expanded by including additional zero terms for size consistency purposes. Additionally, the following definition for $\bar{\mathbf{P}}$ vector is utilized

$$\bar{\mathbf{P}}=\begin{pmatrix}\mathbf{P}^{\mathrm{T}} & \boldsymbol{\Phi}_1^{\mathrm{T}} & \boldsymbol{\Phi}_3^{\mathrm{T}} & \mathbf{P}^{i\mathrm{T}}\end{pmatrix}^{\mathrm{T}} \tag{29}$$

It should be mentioned that difference between $\bar{\mathbf{P}}$ and $\mathbf{P}_{\mathrm{I}}$ vectors are merely the additional pressure degrees of freedom in $\mathbf{P}^{\mathrm{T}}$ part of the former vector (i.e., it includes all nodes in the reservoir domain except the ones at the impounding water surface (i.e., Γ_{IV})). Moreover, it is now apparent based on Eq. (28) that the proposed approach is suitable for transient analysis. However, let us simplify this relation for time harmonic analysis which is the main scope of present study. Under these circumstances, one may write Eq. (28) as follows

$$\begin{pmatrix}-\omega^2\mathbf{M}+(1+2\beta_d\mathrm{i})\mathbf{K} & -\bar{\mathbf{B}}^{\mathrm{T}}\\ -\omega^2\bar{\mathbf{B}} & -\omega^2(\bar{\mathbf{G}}+\bar{\mathbf{M}}_{\mathrm{I}})+\mathrm{i}\omega(q\bar{\mathbf{L}}_{\mathrm{II}}+\bar{\mathbf{C}}_{\mathrm{I}})+(\bar{\mathbf{H}}+\bar{\mathbf{K}}_{\mathrm{I}})\end{pmatrix}\begin{pmatrix}\mathbf{r}\\ \bar{\mathbf{P}}\end{pmatrix}=\begin{pmatrix}-\widetilde{\mathbf{M}}\,\mathbf{J}\,\mathbf{a}_{\mathrm{g}}\\ -\bar{\bar{\mathbf{B}}}\,\mathbf{J}\,\mathbf{a}_{\mathrm{g}}+\bar{\mathbf{F}}_{\mathrm{I}}\end{pmatrix} \tag{30}$$

In this relation, it is assumed that the damping matrix of the dam is of hysteretic type. This means

$$\mathbf{C}=(2\,\beta_d/\omega)\mathbf{K} \tag{31}$$

5. Modeling and basic parameters

The introduced methodology is employed to analyze the Pine Flat dam-reservoir system. This particular dam was selected, because many researchers have analyzed it based on different approaches (Chopra, *et al.* 1980, Feltrin, *et al.* 1990, Lotfi 2002). The dam is 121.92 m high with the crest length of 560.83 m and it is located on the King's River near Fresno, California.

The details about modeling aspects such as discretization, basic parameters and the assumptions adopted are summarized in this section.

5.1 Models

Two-dimensional model of Pine Flat dam-reservoir system is considered on a rigid base. The dam is discretized by 40 isoparametric 8-node plane-solid finite elements in plane-stress state. As for the water domain, two strategies are adopted as explained below (Fig. 2):

For the FE-(FE-TE) method of analysis which is our main procedure, the reservoir near-field is discretized by fluid finite elements and the absorbing boundary condition is employed on the upstream truncation boundary according to different alternatives discussed. This latter task is actually carried out by utilizing a truncation-element at that boundary. The length of this near-field region is denoted by L and water depth is referred to as H. Two normalized reservoir length is considered herein. These are in particular; L/H=1 and 3. Herein, discretization corresponding to the lower length (i.e., L/H=1) is depicted in which 45 isoparametric 8-node plane-fluid finite elements are employed for modeling of the water region (Fig. 2). For the FE-(FE-HE) method of analysis, the reservoir domain is divided into two regions. The near-field region (L/H=1) is discretized by fluid finite elements, and the far-field is treated by a fluid hyper-element (Fig. 2(b)). Of course, it should be emphasized that this option is merely utilized to obtain the exact solutions (Lotfi 2001b, Lotfi 2004). Moreover, it is well-known that the results are not sensitive in this case to the length of the reservoir near-field region or L/H value.

Furthermore, for each case two alternatives are considered which correspond to full reflective (i.e., $\alpha = 1$) and absorptive (i.e., $\alpha = 0.75$) reservoir bottom conditions.

The evaluation of mixed HO-WN condition for different alternatives, are initially carried out for time harmonic analysis. Subsequently, the investigation is performed for transient analysis by considering earthquake excitations.

5.2 Basic parameters

The concrete is assumed to be homogeneous and isotropic with the following basic properties:

Elastic modulus E_c=22.75 GPa.
Poisson's ratio ν_c=0.20
Unit weight γ_c=24.8 kN/m^3
Hysteretic damping factor $\beta_d = 0.05$ (Utilized for time harmonic analysis)

The water is taken as compressible, inviscid fluid, with weight density of 9.81 kN/m^3 and pressure wave velocity of 1440.0 m/s. The water level is considered at the height of 116.19 m above the base, similar to the reference (Chopra, *et al.* 1980).

As mentioned, two different analysis types are carried out. These are time harmonic as well as transient type of analyses. For the former part, the hysteretic damping factor mentioned above is utilized. However, in the latter part, the Rayleigh damping matrix is applied and the

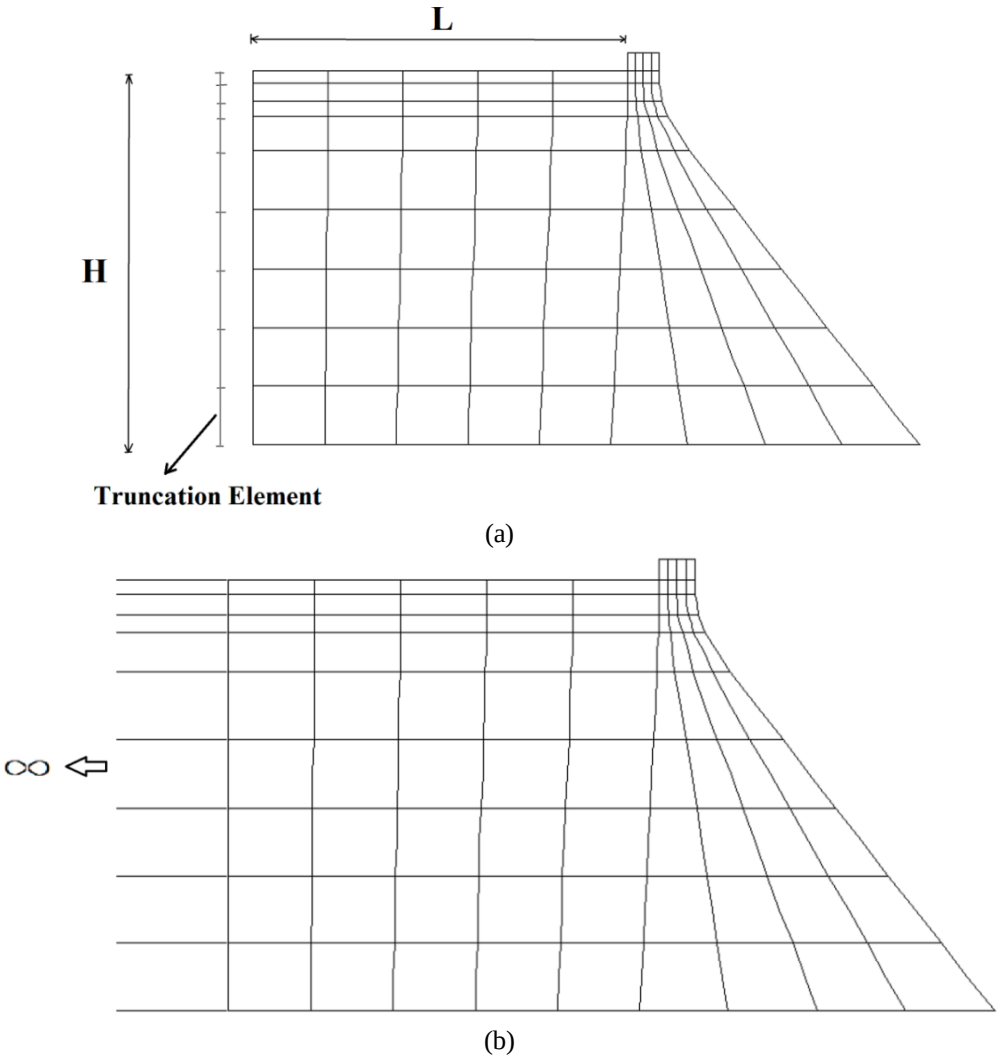

Fig. 2 The dam-reservoir discretization for *L/H*=1; (a) FE-(FE-TE) model, (b) FE-(FE-HE) model

corresponding coefficients are determined such that equivalent damping for frequencies close to the first and tenth modes of vibration corresponding to dam-reservoir system (i.e., $f_1 = 2.545$ Hz and $f_{10} = 8.690$ Hz) would be 5% of the critical damping.

As for mixed HO-WN truncation element, the following properties are utilized:

$\tilde{\omega} = 16.0$ rad/sec

$\tilde{\lambda}_1 = (0.13519\text{E}-1, 0.0)$; full reflective reservoir bottom condition ($\alpha = 1$)

$\tilde{\lambda}_1 = (0.13594\text{E}-1, 0.100395\text{E}-2)$; absorptive reservoir bottom condition ($\alpha = 0.75$)

$\beta = 11\ \bar{c}$

This latter value is selected by a calibration strategy mentioned for the analysis of gravity dams (Samii and Lotfi 2012).

5.3 Loading

For time harmonic analysis, the loading is merely ground motions. However, for transient analysis, it includes both static and dynamic type of loading. It should be mentioned that static loads (weight, hydrostatic pressures) are each visualized as being applied in one separate increment of time. Therefore, the same time step of 0.01 second, which is chosen in dynamic analysis, is also considered as time increment of static loads application. It is noted that time for static analysis is just a convenient tool for applying the load sequentially. However, it is obvious that inertia and damping effects are disregarded in the process. In this respect, the dead load is applied in one increment and hydrostatic pressures thereafter in another increment at negative range of time. At time zero, the actual dynamic analysis begins with the static displacements and stresses being applied as initial conditions. The dynamic excitation considered, is the S69E or vertical component of Taft earthquake records, which is applied in the horizontal or vertical directions separately, along with static loading mentioned. The time duration utilized, is 13 seconds in each case.

6. Results

The initial part of study focuses on the time harmonic analysis of Pine Flat dam-reservoir system. Subsequently, the transient type of analysis will be presented.

6.1 Time harmonic analysis

It should be emphasized that all results presented herein, are obtained by the FE-(FE-TE) method discussed. These are under different absorbing conditions (mixed HO-WN (Alt.1, 2 and 3)) applied on the truncation boundary. The only exception is for what are referred to as the exact responses. Those special cases are carried out by the FE-(FE-HE) analysis technique (Lotfi 2004). The study covers both full reflective and absorptive reservoir bottom condition (i.e., $\alpha = 1$ and 0.75). Moreover, two normalized reservoir lengths are considered as mentioned previously. These are in particular; *L/H*=1 and 3.

For each combination, transfer functions for the horizontal acceleration at dam crest with respect to horizontal or vertical ground acceleration are presented for the three alternatives (Figs. 3-6). It is noted that response in each case is plotted versus the dimensionless frequency. The normalization of excitation frequency is carried out with respect to ω_1 (i.e., $\omega_1 = 19.77$ rad/sec), which is defined as the natural frequency of the dam with an empty reservoir on rigid foundation. Moreover, it is noticed that all cases are compared with its corresponding exact response.

Let us first consider the *L/H*=1 and $\alpha = 1$ combination (Fig. 3). The results for the three alternatives are presented for both horizontal and vertical ground motions. For Alt.1 and 3, it is observed that responses are very accurate up to the second cut-off frequency of the reservoir (i.e., second sharp peak apparent in vertical excitation). This is true for both horizontal and vertical excitation cases. It is also noticed that some kind of noise or distortion exist in the response for higher frequencies after the second cut-off frequency of the reservoir. As for Alt. 2 case, the responses are very similar to the two other cases with the exception that some kind of noise or distortion also exists in the responses right after the first cut-off frequency of the reservoir. This is mainly due to the fact that only one propagating wave term is utilized for this alternative.

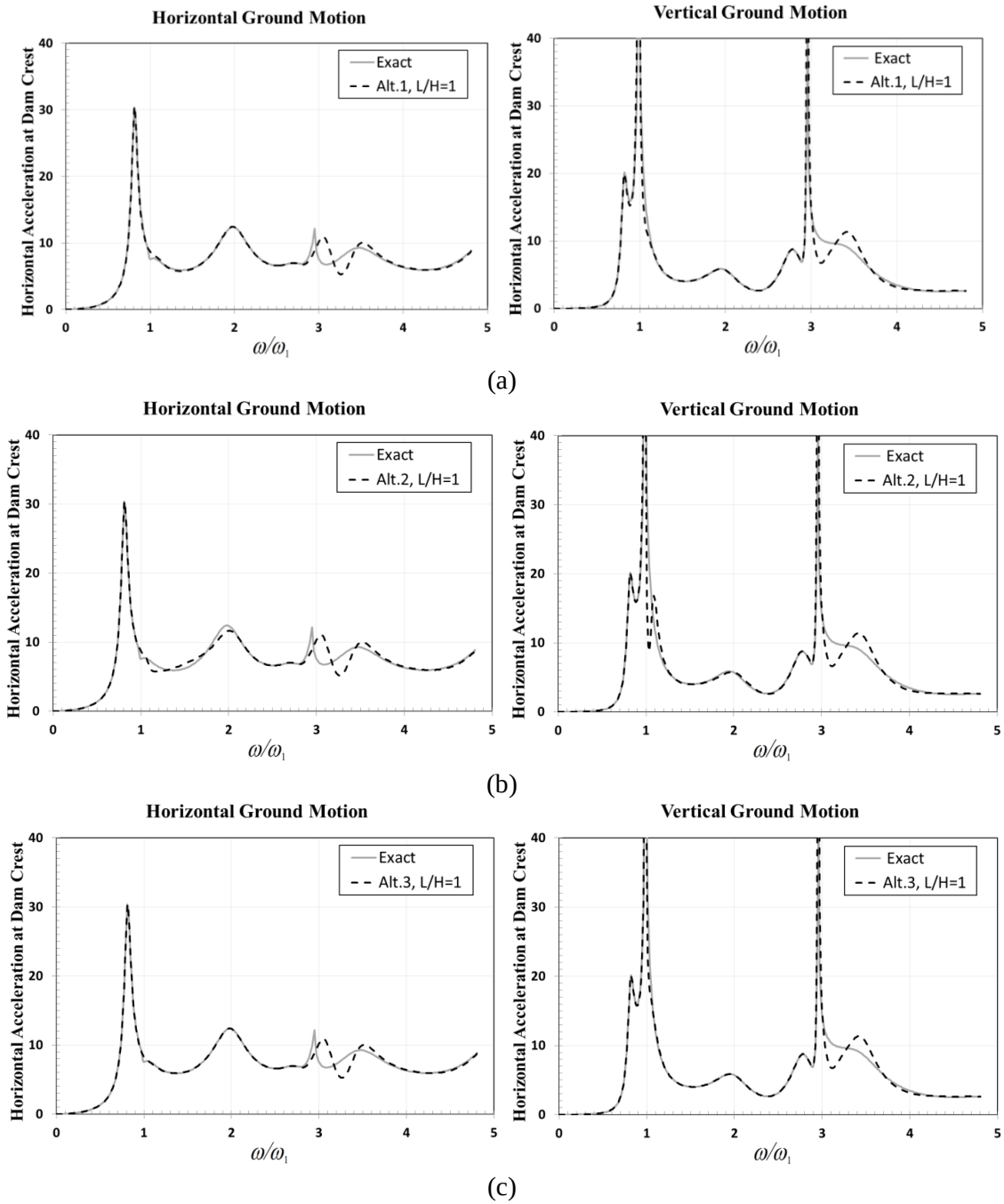

Fig. 3 Horizontal acceleration at dam crest for different alternatives (L/H=1 and $\alpha = 1$); (a) Alt.1, (b) Alt.2, (c) Alt.3

For the L/H=3 and $\alpha = 1$ combination (Fig. 4), trends are similar to previous combination. However, the accuracy is even further improved and errors are reduced. Especially for the

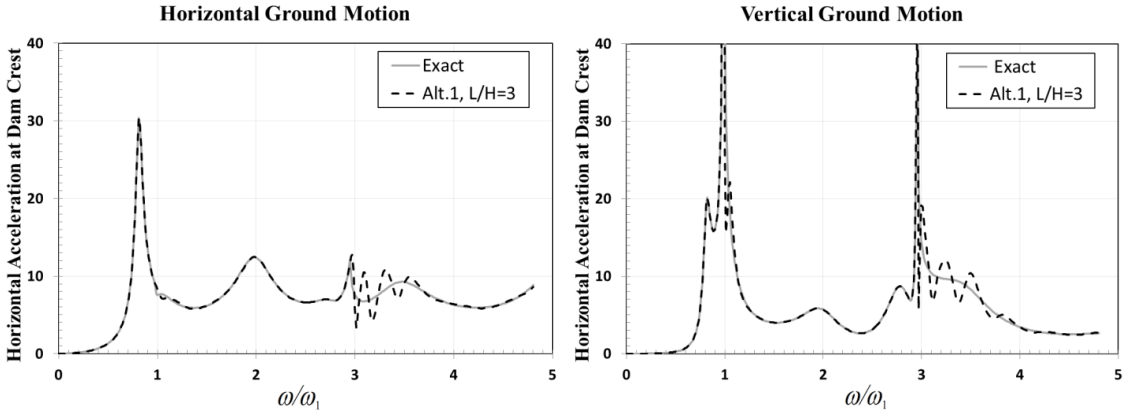

(a)

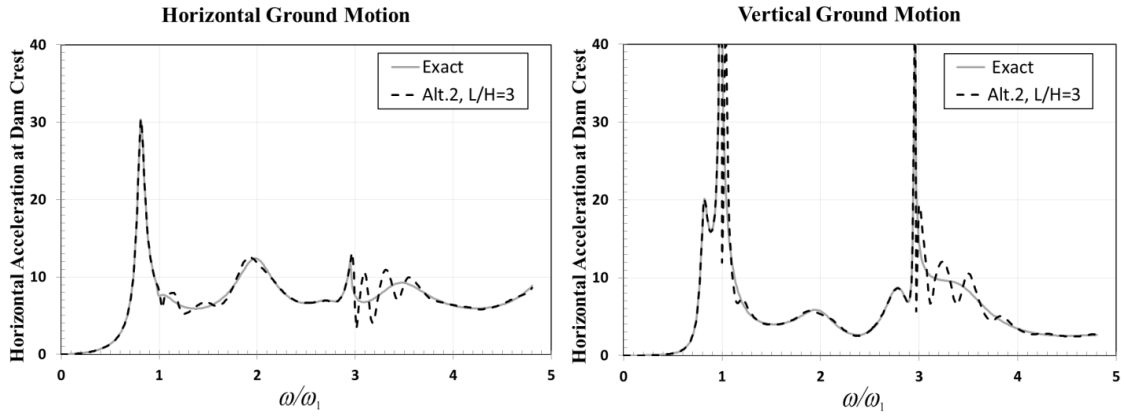

(b)

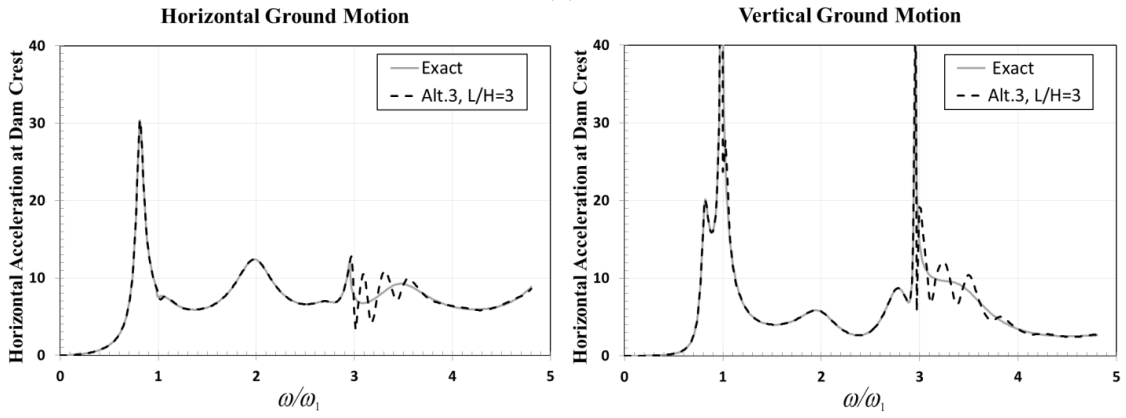

(c)

Fig. 4 Horizontal acceleration at dam crest for different alternatives (L/H=3 and $\alpha = 1$); (a) Alt.1, (b) Alt.2, (c) Alt.3

distortion which was noticed right after the first cut-off frequency of the reservoir in the case of Alt. 2.

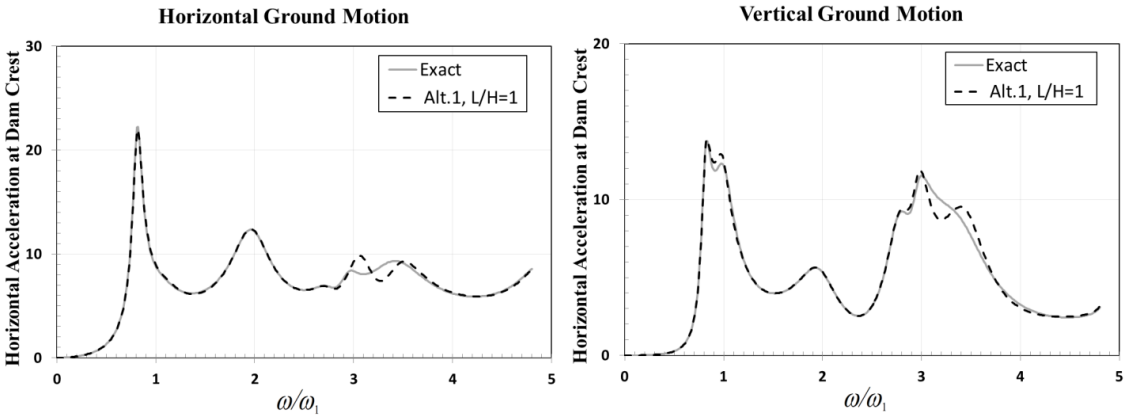

(a)

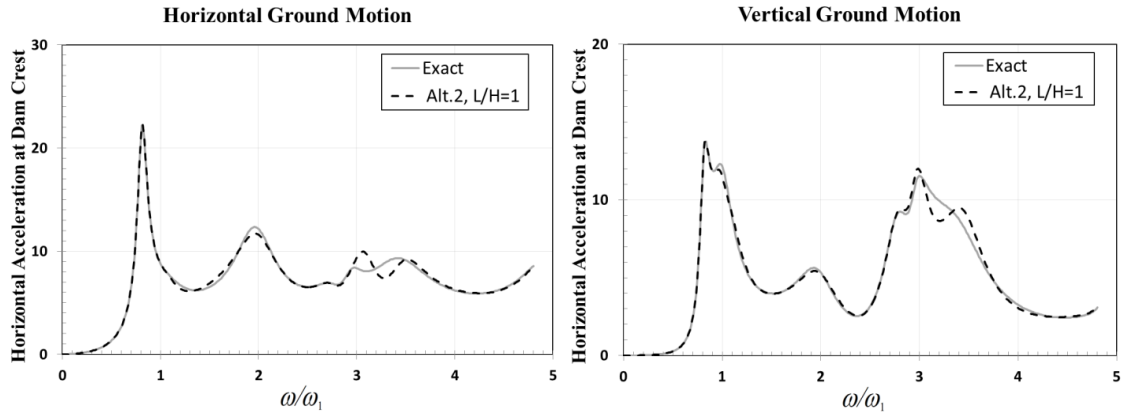

(b)

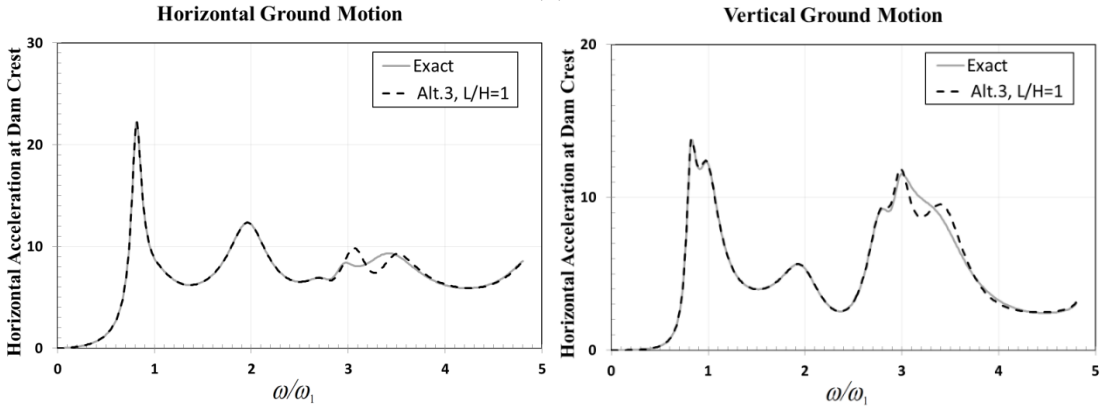

(c)

Fig. 5 Horizontal acceleration at dam crest for different alternatives (*L/H*=1 and $\alpha = 0.75$); (a) Alt.1, (b) Alt.2, (c) Alt.3

For the *L/H*=1 and $\alpha = 0.75$ combination (Fig. 5), trends are similar to *L/H*=1 and $\alpha = 1$ combination (Fig. 3). However, distortions are reduced after the second cut-off frequency of the

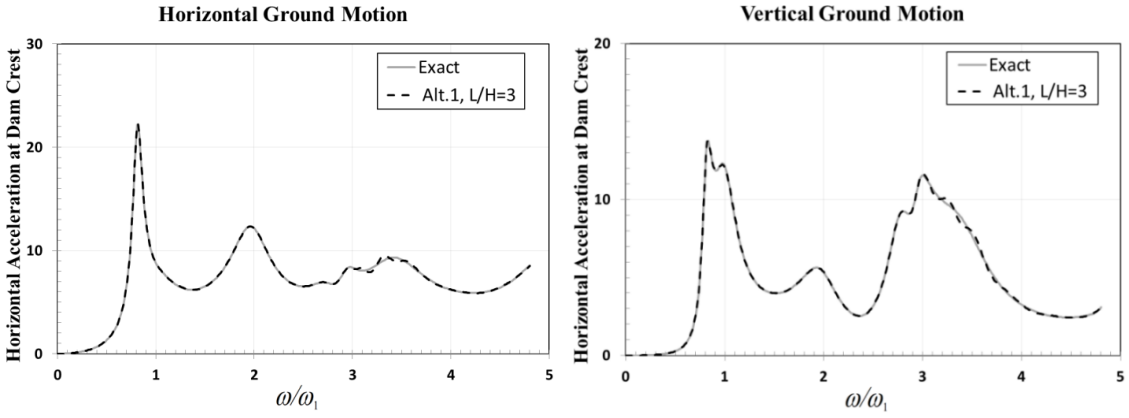

(a)

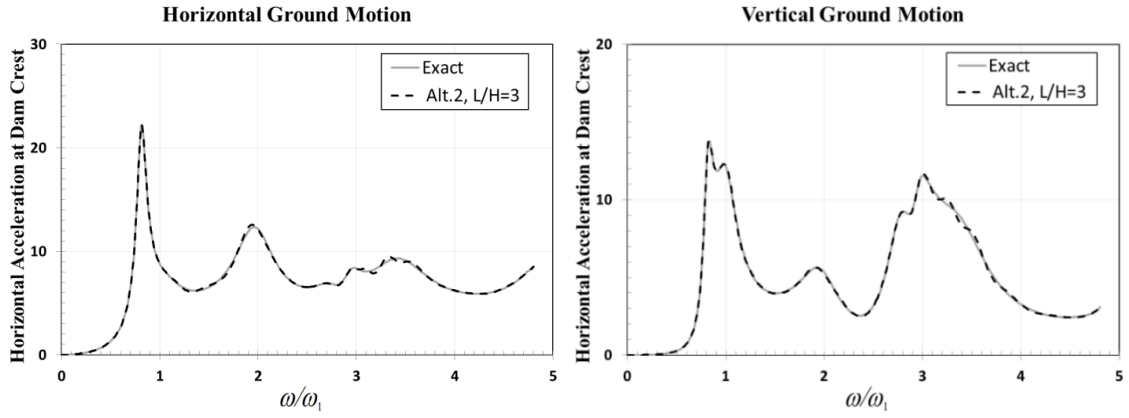

(b)

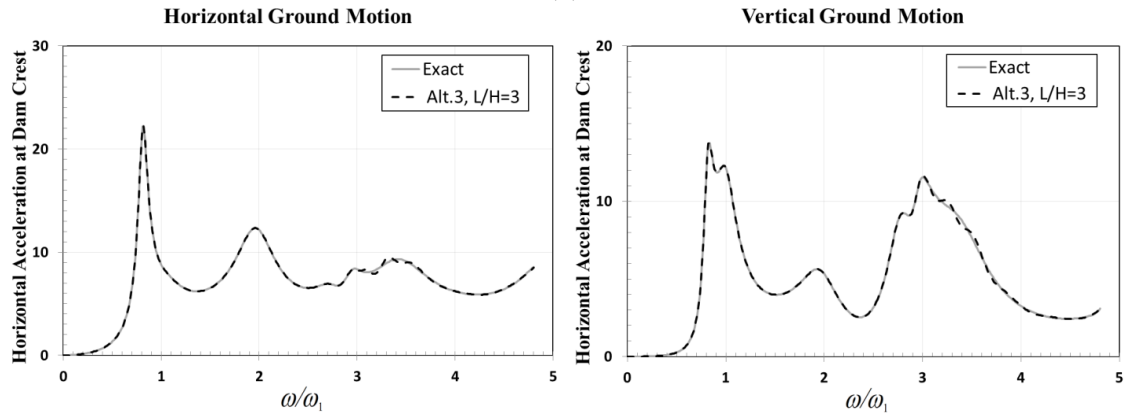

(c)

Fig. 6 Horizontal acceleration at dam crest for different alternatives (L/H=3 and $\alpha = 0.75$); (a) Alt.1, (b) Alt.2, (c) Alt.3

reservoir for all three alternatives. Obviously, this is as a result of additional damping introduced due to absorptive reservoir bottom. Moreover, the distortion is also diminished for Alt. 2 case

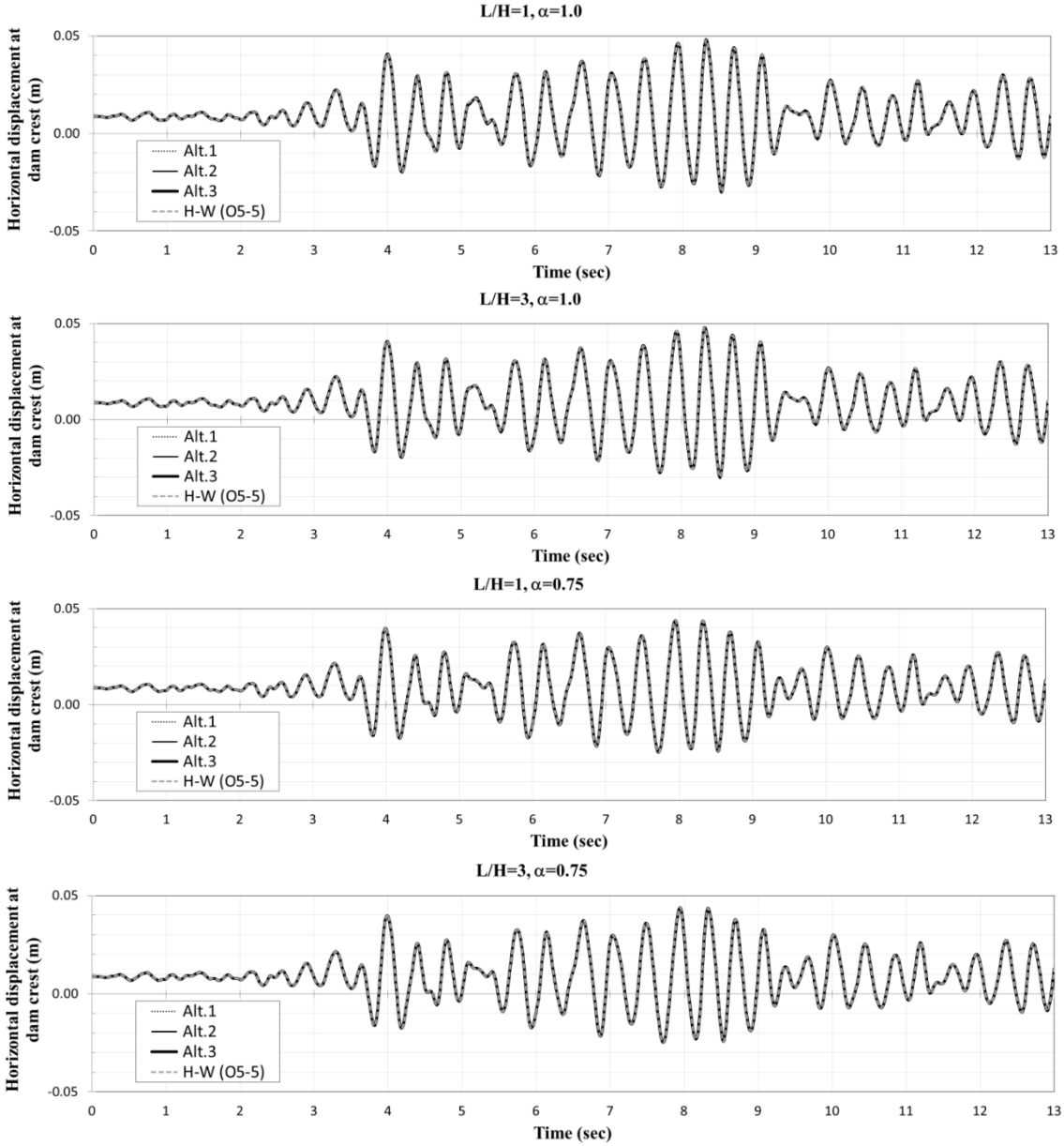

Fig. 7 Comparison of horizontal displacement at dam crest due to horizontal ground motion for different conditions

which was noticeable right after the first cut-off frequency of the reservoir.

As for the *L/H*=3 and $\alpha = 0.75$ combination (Fig. 6), trends are similar to *L/H*=1 and $\alpha = 0.75$ combination (Fig. 5). However, the accuracy is even further improved and errors are reduced. It is such that there are perfect agreements up to the second cut-off frequency of the reservoir and there are minor errors after that. This is true for all three alternatives.

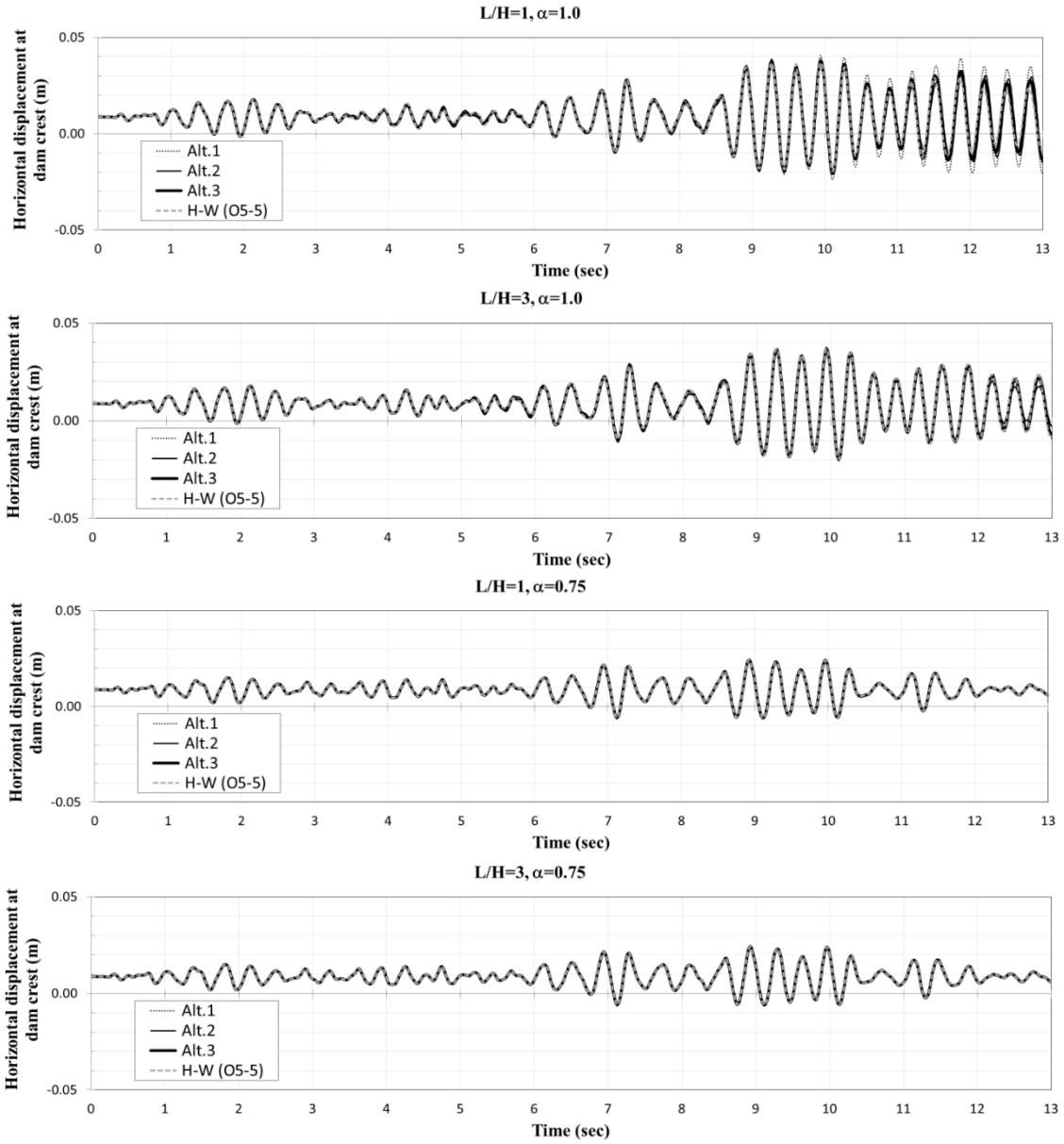

Fig. 8 Comparison of horizontal displacement at dam crest due to vertical ground motion for different conditions

6.2 Transient analysis

It is worthwhile to emphasize that all results presented in this sub-section are mainly obtained by the FE-(FE-TE) method discussed, under different mixed HO-WN (Alt.1, 2 and 3) conditions applied on the truncation boundary. However, the results in each case are compared against the corresponding results obtained by the high order H-W condition (e.g., O5-5) applied on the

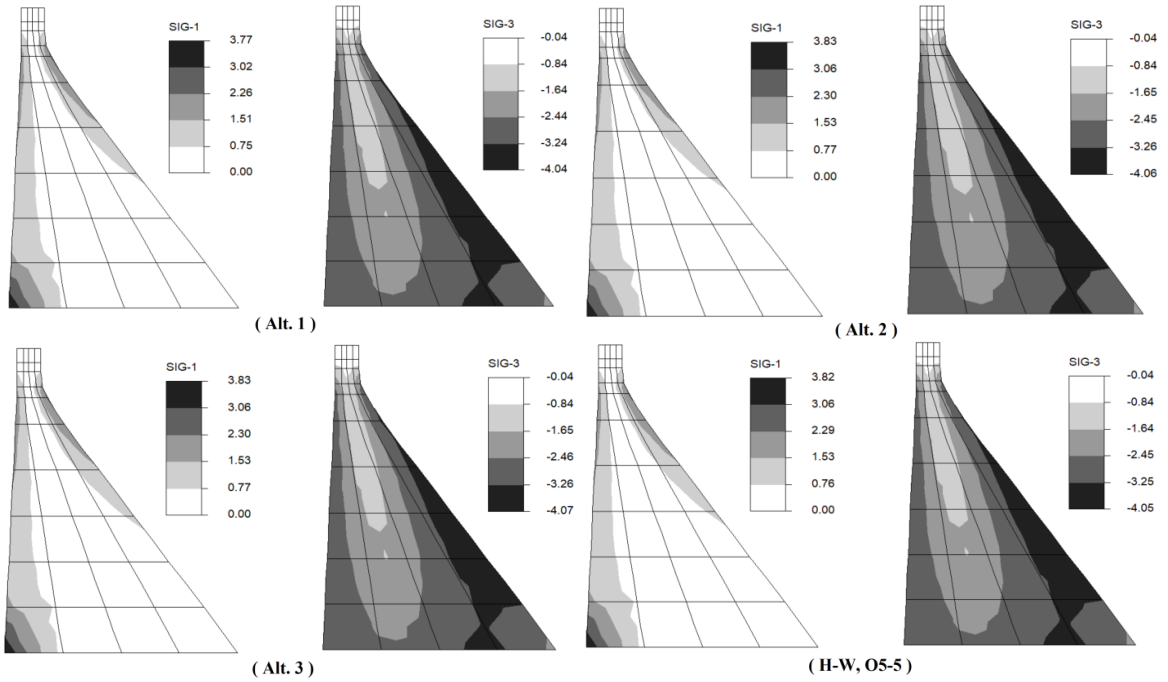

Fig. 9 Comparison of envelope of principal stresses due to horizontal excitation for mixed HO-WN (Alt.1, 2 and 3) and *H-W* (Full reflective reservoir bottom condition (α=1.0) and *L/H*=1)

truncation boundary. This is due to the fact FE-(FE-HE) approach utilized in previous sub-section (referred to as exact method) is merely applicable for frequency domain analysis. It is worthwhile to mention that results for high order H-W condition are not sensitive to *L/H* value. Therefore, they can be envisaged as exact results (in numerical sense) in time domain.

Similar to time harmonic analysis, the study herein covers both full reflective and absorptive reservoir bottom condition (i.e., $\alpha = 1$ and 0.75). Moreover, two normalized reservoir lengths are considered as mentioned previously. These are in particular; *L/H*=1 and 3. Moreover, the dynamic excitation considered, is the S69E or vertical component of Taft earthquake records, which is applied in the horizontal or vertical directions separately, along with static loading mentioned previously.

Let us concentrate initially on the results for time history of horizontal displacement at dam crest which are presented in Figs. 7 and 8. For horizontal excitation, it is observed that there are perfect agreements (Fig. 7) between mixed HO-WN (Alt.1, 2 and 3) responses and the one related to high order H-W (O5-5) for all considered combinations. As for vertical excitation (Fig. 8), it is observed that for *L/H*=1 and $\alpha = 1$ combination (i.e., most challenging condition), there are noticeable errors for Alt.1 and Alt.2 at the latter part of time history. However, even for this condition, the errors for Alt. 3 case are minor. For *L/H*=3 and $\alpha = 1$ combination, the errors decrease significantly for the first two alternatives and there is almost perfect agreement for Alt.3 results. For combinations with $\alpha = 0.75$ (*L/H*=1 or 3), there are again perfect agreements between mixed HO-WN (Alt.1, 2 and 3) responses and the one related to high order H-W (O5-5).

Subsequently, comparisons for envelope of maximum and minimum principal stresses are illustrated between mixed HO-WN (Alt.1, 2 and 3) responses and the one related to high order H-

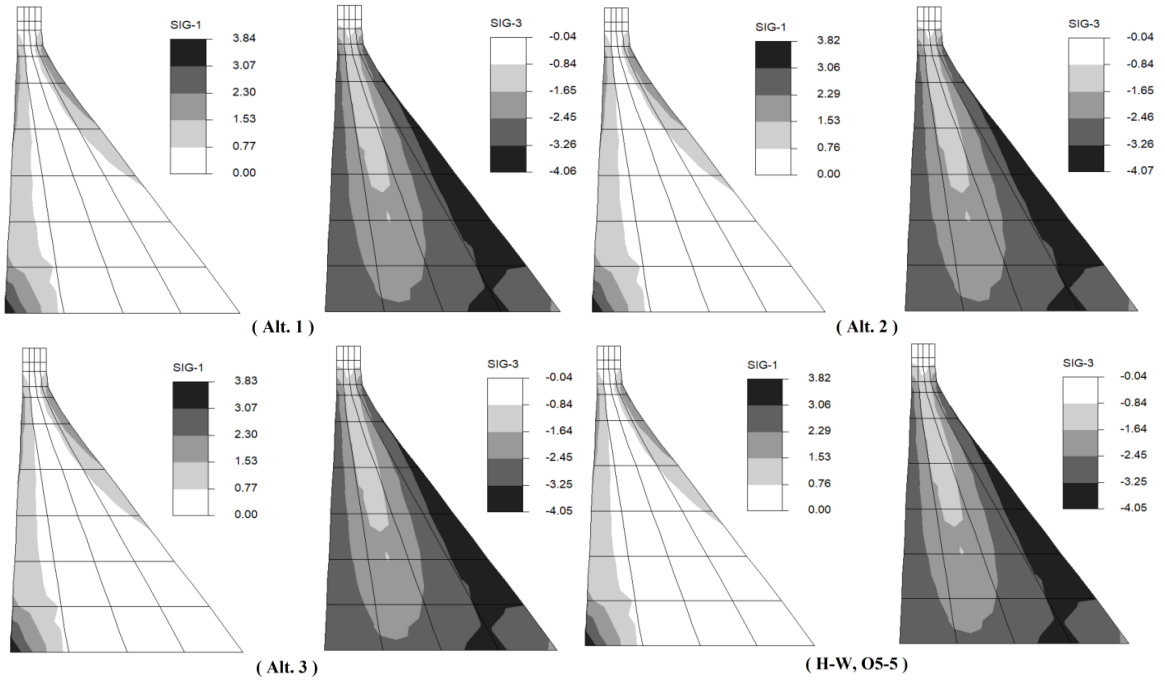

Fig. 10 Comparison of envelope of principal stresses due to horizontal excitation for mixed HO-WN (Alt.1, 2 and 3) and H-W (Full reflective reservoir bottom condition (α=1.0) and L/H=3)

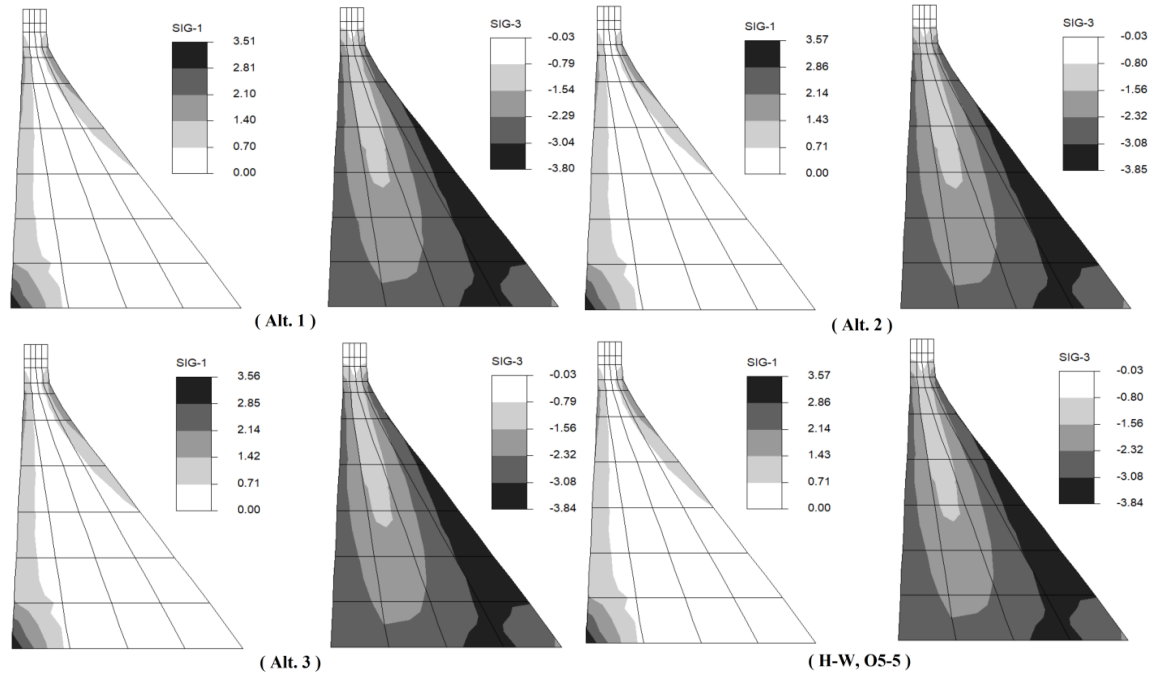

Fig. 11 Comparison of envelope of principal stresses due to horizontal excitation for mixed HO-WN (Alt.1, 2 and 3) and H-W (Absorptive reservoir bottom condition (α=0.75) and L/H=1)

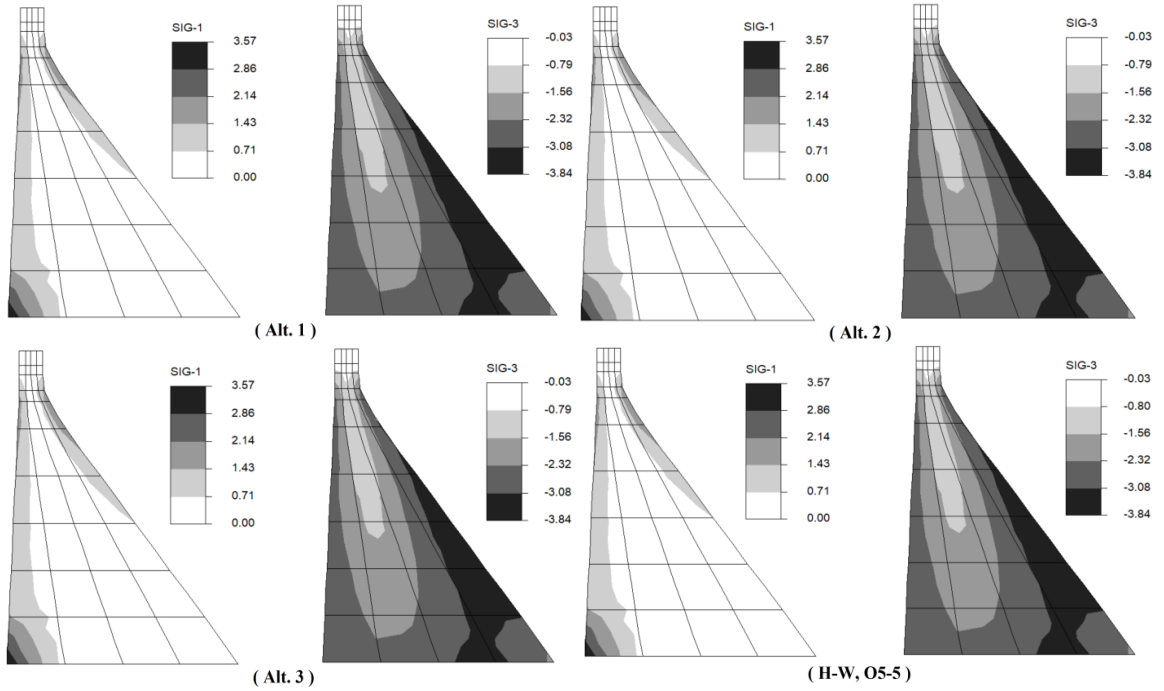

Fig. 12 Comparison of envelope of principal stresses due to horizontal excitation for mixed HO-WN (Alt.1, 2 and 3) and H-W (Absorptive reservoir bottom condition (α=0.75) and L/H=3)

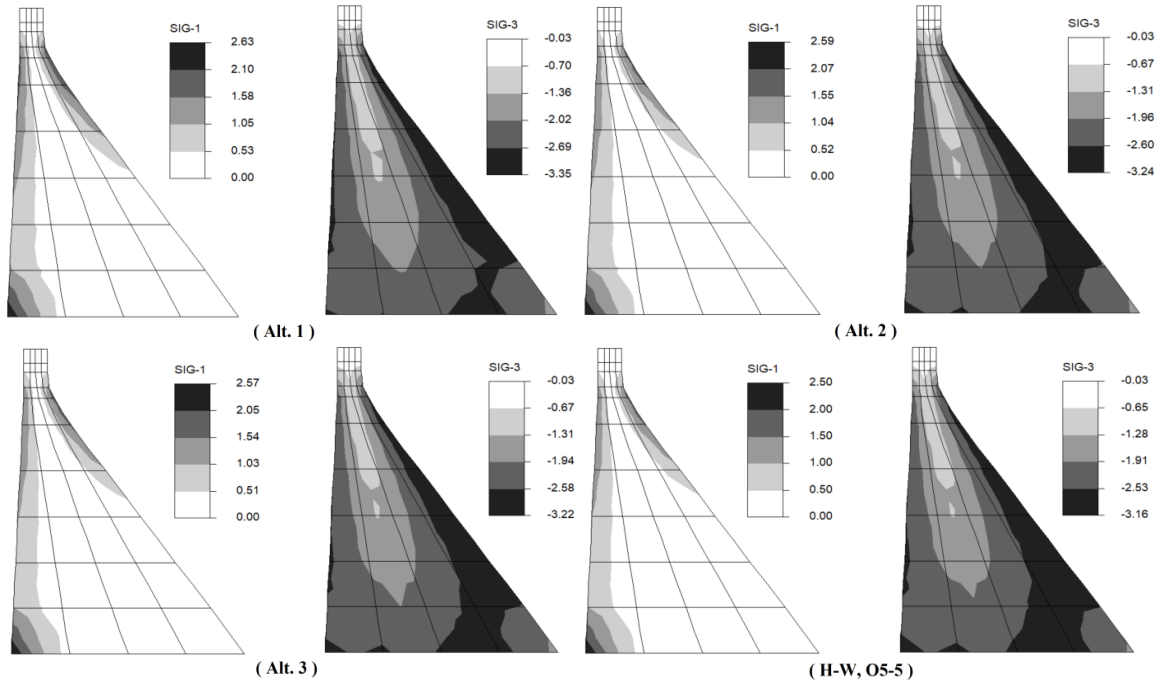

Fig. 13 Comparison of envelope of principal stresses due to vertical excitation for mixed HO-WN (Alt.1, 2 and 3) and H-W (Full reflective reservoir bottom condition (α=1.0) and L/H=1)

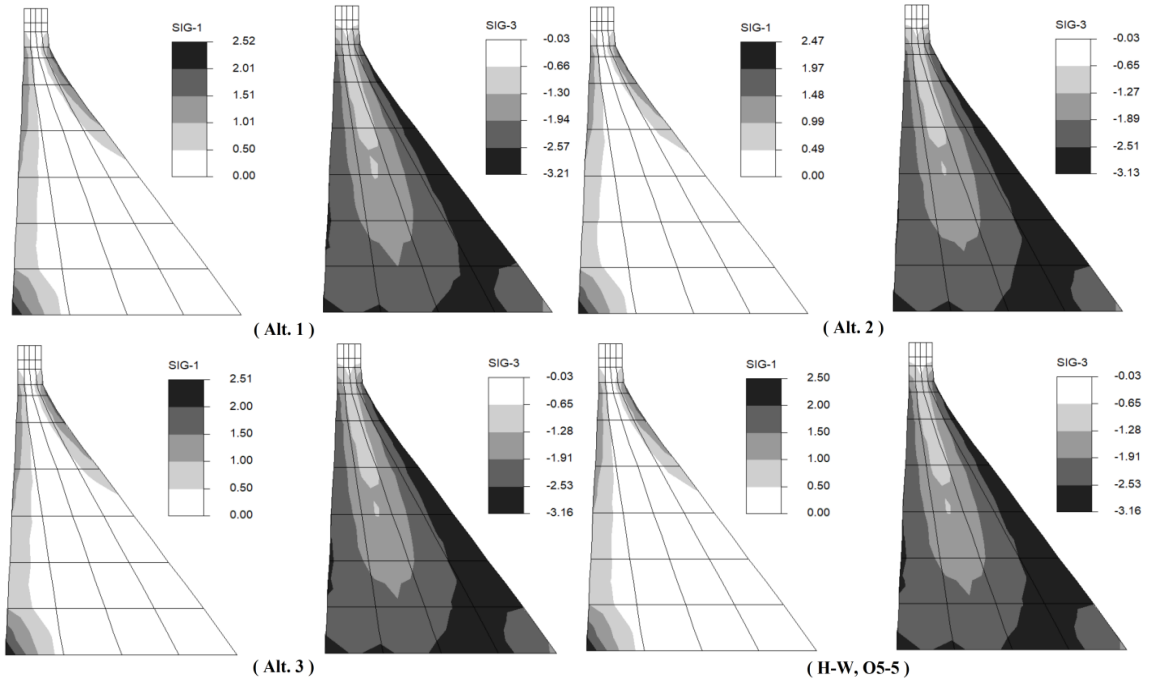

Fig. 14 Comparison of envelope of principal stresses due to vertical excitation for mixed HO-WN (Alt.1, 2 and 3) and H-W (Full reflective reservoir bottom condition (α=1.0) and L/H=3)

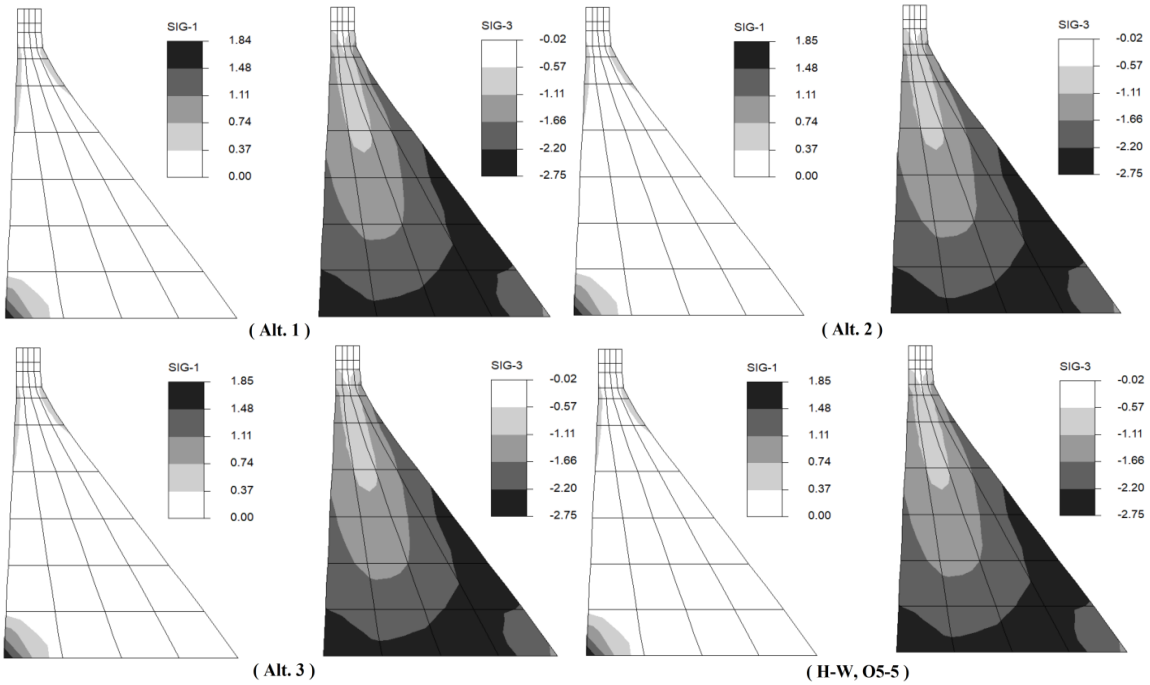

Fig. 15 Comparison of envelope of principal stresses due to vertical excitation for mixed HO-WN (Alt.1, 2 and 3) and H-W (Absorptive reservoir bottom condition (α=0.75) and L/H=1)

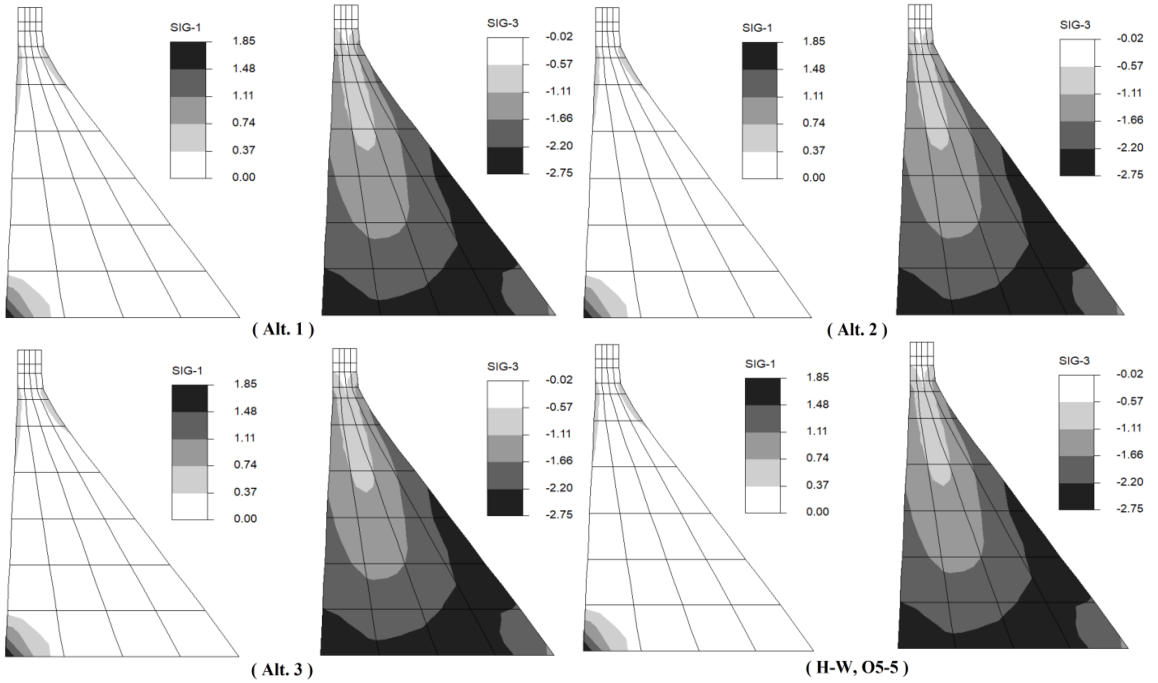

Fig. 16 Comparison of envelope of principal stresses due to vertical excitation for mixed HO-WN (Alt.1, 2 and 3) and H-W (Absorptive reservoir bottom condition (α=0.75) and L/H=3)

Table 5 Maximum and minimum principal stresses due to horizontal excitation

α	L/H	Approach	σ_1 (MPa)	Error for σ_1 (%)	σ_3 (MPa)	Error for σ_3 (%)
1	1	Alt.1	3.77	1.31	-4.04	0.25
		Alt.2	3.83	0.26	-4.06	0.25
		Alt.3	3.83	0.26	-4.07	0.49
		H-W	3.82	-----	-4.05	-----
1	3	Alt.1	3.84	0.52	-4.06	0.25
		Alt.2	3.82	0.00	-4.07	0.49
		Alt.3	3.83	0.26	-4.05	0.00
		H-W	3.82	-----	-4.05	-----
0.75	1	Alt.1	3.51	1.68	-3.80	1.04
		Alt.2	3.57	0.00	-3.85	0.26
		Alt.3	3.56	0.28	-3.84	0.00
		H-W	3.57	-----	-3.84	-----
0.75	3	Alt.1	3.57	0.00	-3.84	0.00
		Alt.2	3.57	0.00	-3.84	0.00
		Alt.3	3.57	0.00	-3.84	0.00
		H-W	3.57	-----	-3.84	-----

Table 6 Maximum and minimum principal stresses due to vertical excitation

α	L/H	Approach	σ_1 (MPa)	Error for σ_1 (%)	σ_3 (MPa)	Error for σ_3 (%)
1	1	Alt.1	2.63	5.20	-3.35	6.01
		Alt.2	2.59	3.60	-3.24	2.53
		Alt.3	2.57	2.80	-3.22	1.90
		H-W	2.50	-----	-3.16	-----
1	3	Alt.1	2.52	0.80	-3.21	1.58
		Alt.2	2.47	1.20	-3.13	0.95
		Alt.3	2.51	0.40	-3.16	0.00
		H-W	2.50	-----	-3.16	-----
0.75	1	Alt.1	1.84	0.54	-2.75	0.00
		Alt.2	1.85	0.00	-2.75	0.00
		Alt.3	1.85	0.00	-2.75	0.00
		H-W	1.85	-----	-2.75	-----
0.75	3	Alt.1	1.85	0.00	-2.75	0.00
		Alt.2	1.85	0.00	-2.75	0.00
		Alt.3	1.85	0.00	-2.75	0.00
		H-W	1.85	-----	-2.75	-----

W (O5-5) case for different conditions (Figs. 9-16). Moreover, maximum value of σ_1 and minimum value of σ_3 are presented for both horizontal and vertical excitations (Tables 5 and 6). The percentages of error are also provided in these Tables for these quantities for a better capture of errors involved in each case.

Let us concentrate first on the results for horizontal excitation. Based on Figs. 9-12 and Table 5, it is observed that results for mixed HO-WN (Alt.1, 2 and 3) and the one related to H-W (O5-5) case for different conditions agree very well. It is such that maximum errors for σ_1 and σ_3 are 1.68 and 1.04 percent, respectively. In regard to vertical excitation, based on Figs. 13-16 and Table 6, it is noticed that error increases in certain cases in comparison with horizontal excitation. However, results still agree quite well. It is such that maximum errors for σ_1 and σ_3 are 5.20 and 6.01 percent, respectively and it corresponds to Alt.1 case for the most challenging considered condition (L/H=1 and $\alpha = 1$ combination).

7. Conclusions

The formulation based on FE-(FE-TE) procedure, was examined for dynamic analysis of a realistic concrete gravity dam-reservoir system. The core of the method is based on utilizing a truncation-element at the upstream truncation boundary of the reservoir near-field domain and excluding far-field region of the reservoir. This truncation-element is formulated based on mixed HO-WN condition applied at that boundary. Three alternatives were discussed for this approach. The first two alternatives result in one additional degree of freedom at each node in comparison with usual modeling in practice which employs Sommerfeld truncation condition. While, the third

alternative leads to two additional degrees of freedom.

A special purpose finite element program (Lotfi 2001a) was enhanced for this investigation. Thereafter, the response of Pine Flat dam-reservoir system was studied due to horizontal and vertical ground motions for two types of reservoir bottom conditions of full reflective (i.e., $\alpha = 1$) and absorptive (i.e., $\alpha = 0.75$). Moreover, two normalized reservoir lengths were considered. In particular, these were *L/H*=1 and 3 which corresponds to low and high normalized reservoir lengths. It should be emphasized that study was carried out under different mixed HO-WN conditions (i.e., Alt.1, 2 and 3) applied on the truncation boundary.

The initial part of study was focused on the time harmonic analysis. In this part, it was possible to compare the transfer functions against corresponding responses obtained by FE-(FE-HE) approach (referred to as exact method). Subsequently, the transient analysis is carried out. In that part, the results in each case are compared against the corresponding results obtained by the high order H-W condition (e.g., O5-5) applied on the truncation boundary. It is worthwhile to emphasize that results for high order H-W condition (e.g., O5-5) are not sensitive to *L/H* value. Therefore, they can be envisaged as exact results (in numerical sense) in time domain. In this respect, the dynamic excitation considered, is the S69E or vertical component of Taft earthquake records, which is applied in the horizontal or vertical directions separately, along with static loading mentioned.

Overall, the main conclusions obtained by the present study can be listed as follows:

Time harmonic analysis

• Under the most challenging considered combination (*L/H*=1 and $\alpha = 1$), it is observed that responses (i.e., transfer functions) are very accurate for Alt.1 and 3 up to the second cut-off frequency of the reservoir (i.e., second sharp peak apparent in vertical excitation). This is true for both horizontal and vertical excitation cases. It is also noticed that some kind of noise or distortion exist in the responses for higher frequencies after the second cut-off frequency of the reservoir. As for Alt. 2 case, the responses are very similar to the two other cases with the exception that some kind of noise or distortion also exists in the responses right after the first cut-off frequency of the reservoir. This is mainly due to the fact that only one propagating wave term is utilized for this alternative.

• For other combinations, trends are similar to the challenging combination mentioned. However, the accuracy is even further improved and errors are reduced. It is such that for the most favorable considered combination (*L/H*=3 and $\alpha = 0.75$), there are perfect agreements for the transfer functions up to the second cut-off frequency of the reservoir and there are minor errors after that. This is true for all three alternatives.

Transient analysis

• In regard to time history of horizontal displacement at dam crest due to horizontal excitation, it is observed that there are perfect agreements between mixed HO-WN (Alt.1, 2 and 3) responses and the one related to high order H-W (O5-5) for all considered combinations.

• As for the time history of horizontal displacement at dam crest due to vertical excitation, it is observed that for *L/H*=1 and $\alpha = 1$ combination (i.e., most challenging condition), there are noticeable errors for Alt.1 and Alt.2 at the latter part of time history. However, even for this condition, the errors for Alt. 3 case are minor. For *L/H*=3 and $\alpha = 1$ combination, the errors decrease significantly for the first two alternatives and there is almost perfect agreement for Alt.3 results. For combinations with $\alpha = 0.75$ (*L/H*=1 or 3), there are again perfect agreements between mixed HO-WN (Alt.1, 2 and 3) responses and the one related to high order H-W (O5-5).

• Based on envelope of principal stresses and maximum value of σ_1 and minimum value of σ_3 extracted from these contours, it is observed that results for mixed HO-WN (Alt.1, 2 and 3) and the one related to H-W (O5-5) case agree very well for horizontal excitation under different conditions. It is such that maximum errors for σ_1 and σ_3 are 1.68 and 1.04 percent, respectively.
• In regard to vertical excitation, it is noticed that error increases in certain cases in comparison with horizontal excitation. However, results still agree quite well. It is such that maximum errors for $\sigma_1$and σ_3 are 5.20 and 6.01 percent, respectively and it corresponds to Alt.1 case for the most challenging considered condition (*L/H*=1 and $\alpha = 1$ combination).
• In general, it can be claimed that all three alternatives of mixed HO-WN approach are acting very well and Alt. 3 is most accurate. Of course, it should be emphasized that both Alt.1 and Alt.2 have merely one additional degree of freedom in comparison with usual Sommerfeld truncation condition, while Alt. 3 employs two additional degrees of freedom.

References

Akbari, R. and Lotfi, V. (2022), "Nonlinear dynamic analysis of concrete gravity dams utilizing a simplified continuum damage model and different damping algorithms", *Asian J. Civil Eng.*, **24**(2), 453-468. https://doi.org/10.1007/s42107-022-00511-2.

Akbari, R., Hashempour, S.A. and Lotfi, V. (2023), "Nonlinear seismic evaluation of concrete dams utilizing a simplified isotropic damage model", *Dam Eng.*, **33**(1), 1-25.

Arjmandi, S.A. and Lotfi, V. (2011), "Computing mode shapes of fluid-structure systems using subspace iteration methods", *Scientia Iranica*, **18**(6), 1159-1169. https://doi.org/10.1016/j.scient.2011.09.011.

Arjmandi, S.A. and Lotfi, V. (2013), "Comparison of three efficient methods for computing mode shapes of fluid-structure interaction systems", *Arab. J. Sci. Eng.*, **38**, 787-803. https://doi.org/10.1007/s13369-012-0523-8.

Basu, U. and Chopra, A.K. (2003), "Perfectly matched layers for time-harmonic elastodynamics of unbounded domains: Theory and finite-element implementation", *Comput. Meth. Appl. Mech. Eng.*, **192**(11-12), 1337-1375. https://doi.org/10.1016/S0045-7825(02)00642-4.

Berenger, J.P. (1994), "A perfectly matched layer for the absorption of electromagnetic waves", *J. Comput. Phys.*, **114**(2), 185-200. https://doi.org/10.1006/jcph.1994.1159.

Chew, W.C. and Weedon, W.H. (1994), "A 3D perfectly matched medium from modified Maxwell's equations with stretched coordinates", *Microw. Opt. Techn. Let.*, **7**(13), 599-604. https://doi.org/10.1002/mop.4650071304.

Chopra, A.K. (1967), "Hydrodynamic pressure on dams during earthquake", *J. Eng. Mech.*, **93**, 205-223. https://doi.org/10.1061/JMCEA3.0000915.

Chopra, A.K., Chakrabarti, P. and Gupta, S. (1980), "Earthquake response of concrete gravity dams including hydrodynamic and foundation interaction effects", Report No. EERC-80/01, University of California, Berkeley.

Dehghanmarvasty, S. and Lotfi, V. (2023), "Dynamic analysis of Pine Flat dam-reservoir system utilizing Hagstrom-Warburton truncation boundary condition", *Couple. Syst. Mech.*, **12**(4), 365-389. https://doi.org/10.12989/csm.2023.12.4.365.

Farzad, R. and Lotfi, V. (2023), "Modal analysis of concrete arch dam–reservoir–massed foundation system in frequency domain", *Proc. Inst. Civil Eng.*, **176**(4), 244-256. https://doi.org/10.1680/jstbu.20.00160.

Fenves, G. and Chopra, A.K. (1985), "Effects of reservoir bottom absorption and dam-water-foundation interaction on frequency response functions for concrete gravity dams", *Earthq. Eng. Struct. Dyn.*, **13**, 13-31. https://doi.org/10.1002/eqe.4290130104.

Ganji, H.T. and Lotfi, V. (2021), "Transient analysis of concrete gravity dams by Wavenumber-TD method

for general excitation", *Proc. Inst. Civil Eng. Struct. Build.*, **174**(4), 259-275. https://doi.org/10.1680/jstbu.19.00041.

Givoli, D. and Neta, B. (2003), "High order non-reflecting boundary scheme for time-dependent waves", *J. Comput. Phys*., **186**(1), 24-46. https://doi.org/10.1016/S0021-9991(03)00005-6.

Givoli, D., Hagstrom, T. and Patlashenko, I. (2006), "Finite-element formulation with high-order absorbing conditions for time-dependent waves", *Comput. Meth. Appl. Mech. Eng*., **195**(29-32), 3666-3690. https://doi.org/10.1016/j.cma.2005.01.021.

Hadzalic, E., Ibrahimbegovic, A. and Dolarevic, S. (2018), "Fluid-structure interaction system predicting both internal pore pressure and outside hydrodynamic pressure", *Couple. Syst. Mech.*, **7**(6), 649-668. https://doi.org/10.12989/csm.2018.7.6.649.

Hadzalic, E., Ibrahimbegovic, A. and Dolarevic, S. (2019), "Theoretical formulation and seamless discrete approximation for localized failure of saturated poro-plastic structure interacting with reservoir", *Comput. Struct.*, **214**, 73-93. https://doi.org/10.1016/j.compstruc.2019.01.003.

Hagstrom, T. and Warburton, T. (2004), "A new auxiliary variable formulation of high order local radiation boundary condition: corner compatibility conditions and extensions to first-order systems", *Wave Motion*, **39**(4), 327-338. https://doi.org/10.1016/j.wavemoti.2003.12.007.

Hagstrom, T., Mar-Or, A. and Givoli, D. (2008), "High-order local absorbing conditions for the wave equation: extensions and improvements", *J. Comput. Phys*., **227**, 3322-3357. https://doi.org/10.1016/j.jcp.2007.11.040.

Hall, J.F. and Chopra, A.K. (1982), "Two-dimensional dynamic analysis of concrete gravity and embankment dams including hydrodynamic effects", *Earth. Eng. Struct. Dyn.*, **10**(2), 305-332. https://doi.org/10.1002/eqe.4290100211.

Higdon, R.L. (1986), "Absorbing boundary conditions for difference approximations to the multi-dimensional wave equation", *Math. Comput.*, **47**(176), 437-459. https://doi.org/10.1090/S0025-5718-1986-0856696-4.

Hosseinzadeh, A., Nobarinasab, M., Soroush, A. and Lotfi, V. (2013), "Coupled stress–seepage analysis of Karun III concrete arch dam", *Proc. Inst. Civil Eng.-Geotech. Eng.*, **166**(5), 483-501. https://doi.org/10.1680/geng.10.00119.

Jafari, M. and Lotfi, V. (2018), "Dynamic analysis of concrete gravity dam-reservoir systems by Wavenumber approach for the general reservoir base condition", *Int. J. Sci. Technol. (Scientia Iranica)*, **25**(6), 3054-3065. https://doi.org/10.24200/sci.2017.4227.

Karabulut, M. and Kartal, M.E. (2018), "Seismic analysis of concrete arch dams considering hydrodynamic effect using Westergaard approach", *Sakarya Univ. J. Sci.*, **23**(2), 149-161. https://doi.org/10.16984/saufenbilder.394266.

Khazaee, A. and Lotfi, V. (2014a), "Application of perfectly matched layers in the transient analysis of dam-reservoir systems", *Soil Dyn. Earthq. Eng.*, **60**(1), 51-68. https://doi.org/10.1016/j.soildyn.2014.01.005.

Khazaee, A. and Lotfi, V. (2014b), "Time harmonic analysis of dam-foundation systems by perfectly matched layers", *Struct. Eng. Mech.*, **50**(3), 349-364. https://doi.org/10.12989/sem.2014.50.3.349.

Kim, S. and Pasciak J.E. (2012), "Analysis of cartesian PML approximation to acoustic scattering problems in R2", *Wave Motion*, **49**, 238-257. https://doi.org/10.1016/j.jmaa.2010.05.006.

Liu, J., Ma, J.W. and Yang, H.Z. (2009), "The study of perfectly matched layer absorbing boundaries for SH wave fields", *Appl. Geophys*., **6**(3), 267-274. https://doi.org/10.1007/s11770-009-0023-0.

Lokke, A. and Chopra, A.K. (2017), "Direct finite element method for nonlinear analysis of semi-unbounded dam-water-foundation rock systems", *Earthq. Eng. Struct. Dyn.*, **46**(8), 1267-1285. https://doi.org/10.1002/eqe.2855.

Lokke, A. and Chopra, A.K. (2018), "Direct finite element method for nonlinear earthquake analysis of 3-dimensional semi-unbounded dam-water-foundation rock systems", *Earthq. Eng. Struct. Dyn*., **47**(5), 1309-1328. https://doi.org/10.1002/eqe.3019.

Lotfi, V. (2001a), "MAP-76: A Program for Analysis of Concrete Dams", Department of Civil & Environmental Engineering, Amirkabir University of Technology, Tehran, Iran.

Lotfi, V. (2001b), "Frequency domain analysis of gravity dams including hydrodynamic effects", *Dam Eng.*,

12(1), 33-53.
Lotfi, V. (2004), "Direct frequency domain analysis of concrete arch dams based on FE-(FE-HE)-BE technique", *Comput. Concrete*, **1**(3), 285-302. https://doi.org/10.12989/cac.2004.1.3.285.
Lotfi, V. (2017), "Dynamic analysis of concrete gravity dam-reservoir systems by Wavenumber approach for the general reservoir base condition and ground excitation", *Dam Eng.*, **27**(3), 33-57.
Lotfi, V. and Dehghanmarvasty, S. (2023), "Time harmonic analysis of concrete gravity dam-reservoir systems by mixed High order-Wavenumber approach approach for general reservior bottom condition", *Struct*., **55**, 1906-1919. https://doi.org/10.1016/j.istruc.2023.06.107.
Lotfi, V. and Lotfi, A. (2021), "Application of Hagstrom-Warburton high-order truncation boundary condition on time harmonic analysis of concrete arch dam-reservoir systems", *Eng. Comput.*, **38**(7), 2996-3020. https://doi.org/10.1108/EC-08-2020-0441.
Lotfi, V. and Lotfi, A. (2022), "Time harmonic analysis of concrete arch dam-reservoir systems by utilizing GN high-order truncation condition", *Scientia Iranica*, **29**(6), 2825-2836. https://doi.org/10.24200/sci.2022.57180.5102.
Lotfi, V. and Omidi, O. (2012), "Dynamic analysis of Koyna dam using three-dimensional plastic-damage modeling", *Dam Eng.*, **22**(3), 197-226.
Lotfi, V. and Samii, A. (2012), "Dynamic analysis of concrete gravity dam-reservoir systems by wavenumber approach in the frequency domain", *Earthq. Struct.*, **3**(3-4), 533-548. https://doi.org/10.12989/eas.2012.1.3/4.533.
Lotfi, V. and Sharghi, M.R. (2000), "Earthquake response of concrete gravity dams by combination of finite element and boundary integral formulations", *12th World Conference on Earthquake Engineering*.
Lotfi, V. and Sharghi, M.R. (2001), "Direct frequency domain analysis of concrete gravity dams based on the FE-BE procedure", *Dam Eng.*, **11**(4), 197-226.
Lotfi, V. and Zenz, G. (2016), "Transient analysis of concrete gravity dam-reservoir systems by Wavenumber-TD approach", *Soil Dyn. Earthq. Eng.*, **90**(1), 313-326. https://doi.org/10.1016/j.soildyn.2016.08.026.
Lotfi, V. and Zenz, G. (2018), "Application of Wavenumber-TD approach for time harmonic analysis of concrete arch dam-reservoir systems", *Couple. Syst. Mech.*, **7**(3), 353-371. https://doi.org/10.12989/csm.2018.7.3.353.
Lotfi, V. and Zenz, G. (2022), "Application of Wavenumber-TD approach for transient analysis of concrete arch dam-reservoir systems", *Dam Eng.*, **31**(3), 167-188.
Rabinovich, D., Givoli, D., Bielak, J. and Hagstrom, T. (2011), "A finite element scheme with a high order absorbing boundary condition for elastodynamics", *Comput. Meth. Appl. Mech*., **200**, 2048-2066. https://doi.org/10.1016/j.cma.2011.03.006.
Samii, A. and Lotfi, V. (2012), "High-order adjustable boundary condition for absorbing evanescent modes of waveguides and its application in coupled fluid-structure analysis", *Wave Motion*, **49**(2), 238-257. https://doi.org/10.1016/j.wavemoti.2011.10.001.
Sani, A.A. and Lotfi, V. (2007), "Linear dynamic analysis of arch dams utilizing modified efficient fluid hyper-element", *Eng. Struct.*, **29**(10), 2654-2661. https://doi.org/10.1016/j.engstruct.2007.01.005.
Sani, A.A. and Lotfi, V. (2011), "An effective procedure for seismic analysis of arch dams including dam-reservoir-foundation interaction effects", *Earthq. Eng.*, **15**(7), 971-988. https://doi.org/10.1080/13632469.2010.551703.
Sommerfeld, A. (1949), *Partial Differential Equations in Physics*, Academic Press, NY.
Waas, G. (1972), "Linear two-dimensional analysis of soil dynamics problems in semi-infinite layered media", Ph.D. Dissertation, University of California, Berkeley, California.
Zienkiewicz, O.C., Taylor, R.L. and Zhu, J.Z. (2013), *The Finite Element Method*, Butterworth-Heinemann.

Appendix A. The basic relations for Alt.1

Although, it is much simpler, the basic relations for Alt.1 are as follows

$$\mathbf{L}_{\mathrm{I}}\boldsymbol{\Phi}_1 + \bar{c}\,\mathbf{L}_{\mathrm{I}}\left(\dot{\mathbf{P}} - \dot{\mathbf{P}}^i\right) + \mathbf{R}_{\mathrm{I}}^e = \mathbf{0} \tag{A.1}$$

$$\begin{gathered}-\beta\left(\tilde{\lambda}_1^2\right)^R\mathbf{L}_{\mathrm{I}}\left(\mathbf{P} - \mathbf{P}^i\right) - \tfrac{\beta}{\bar{\omega}}\left(\tilde{\lambda}_1^2\right)^I\mathbf{L}_{\mathrm{I}}\left(\dot{\mathbf{P}} - \dot{\mathbf{P}}^i\right) + \left(\tilde{\lambda}_1^2\right)^R\mathbf{L}_{\mathrm{I}}\boldsymbol{\Phi}_1 + \tfrac{1}{\bar{\omega}}\left(\tilde{\lambda}_1^2\right)^I\mathbf{L}_{\mathrm{I}}\dot{\boldsymbol{\Phi}}_1 - \bar{c}\left(\tilde{\lambda}_1^2\right)^R\mathbf{L}_{\mathrm{I}}\left(\dot{\mathbf{P}} - \right. \\ \left.\dot{\mathbf{P}}^i\right) - \tfrac{\bar{c}}{\bar{\omega}}\left(\tilde{\lambda}_1^2\right)^I\mathbf{L}_{\mathrm{I}}\left(\ddot{\mathbf{P}} - \ddot{\mathbf{P}}^i\right) + 2\beta\bar{c}\,\mathbf{L}_{\mathrm{I}}\dot{\boldsymbol{\Phi}}_1 + 2\bar{c}^2\mathbf{L}_{\mathrm{I}}\ddot{\boldsymbol{\Phi}}_1 = \mathbf{0}\end{gathered} \tag{A.2}$$

$$\bar{c}^2\,\mathbf{L}_{\mathrm{I}}\,\ddot{\mathbf{P}}^i + \mathbf{Q}_{\mathrm{I}}\,\dot{\mathbf{P}}^i + \mathbf{D}_{\mathrm{I}}\,\mathbf{P}^i = -\mathbf{E}_{\mathrm{I}}^i\,\mathbf{a}_g \tag{A.3}$$

Based on these relations, the explicit forms of generalized matrices ($\mathbf{M}_{\mathrm{I}}$, $\mathbf{C}_{\mathrm{I}}$ and $\mathbf{K}_{\mathrm{I}}$) are quite apparent:

Table A.1 Explicit form of generalized matrix $\mathbf{M}_{\mathrm{I}}$ (Alt.1)

	$\mathbf{P}^{\mathrm{T}}$	$\boldsymbol{\Phi}_1^{\mathrm{T}}$	$\mathbf{P}^{i\mathrm{T}}$
$\mathbf{P}$	$\mathbf{0}$	$\mathbf{0}$	$\mathbf{0}$
$\boldsymbol{\Phi}_1$	$-\frac{\bar{c}}{\bar{\omega}}\left(\tilde{\lambda}_1^2\right)^I\mathbf{L}_{\mathrm{I}}$	$2\bar{c}^2\mathbf{L}_{\mathrm{I}}$	$\frac{\bar{c}}{\bar{\omega}}\left(\tilde{\lambda}_1^2\right)^I\mathbf{L}_{\mathrm{I}}$
$\mathbf{P}^i$	$\mathbf{0}$	$\mathbf{0}$	$\bar{\mathrm{c}}^2\mathbf{L}_{\mathrm{I}}$

Table A.2 Explicit form of generalized matrix $\mathbf{C}_{\mathrm{I}}$ (Alt.1)

	$\mathbf{P}^{\mathrm{T}}$	$\boldsymbol{\Phi}_1^{\mathrm{T}}$	$\mathbf{P}^{i\mathrm{T}}$
$\mathbf{P}$	$\bar{\mathrm{c}}\,\mathbf{L}_{\mathrm{I}}$	$\mathbf{0}$	$-\bar{\mathrm{c}}\,\mathbf{L}_{\mathrm{I}}$
$\boldsymbol{\Phi}_1$	$\left(-\frac{\beta}{\bar{\omega}}\left(\tilde{\lambda}_1^2\right)^I - \bar{c}\left(\tilde{\lambda}_1^2\right)^R\right)\mathbf{L}_{\mathrm{I}}$	$\left(+\frac{1}{\bar{\omega}}\left(\tilde{\lambda}_1^2\right)^I + 2\beta\bar{c}\right)\mathbf{L}_{\mathrm{I}}$	$\left(\frac{\beta}{\bar{\omega}}\left(\tilde{\lambda}_1^2\right)^I + \bar{c}\left(\tilde{\lambda}_1^2\right)^R\right)\mathbf{L}_{\mathrm{I}}$
$\mathbf{P}^i$	$\mathbf{0}$	$\mathbf{0}$	$\mathbf{Q}_{\mathrm{I}}$

Table A.3 Explicit form of generalized matrix $\mathbf{K}_{\mathrm{I}}$ (Alt.1)

	$\mathbf{P}^{\mathrm{T}}$	$\boldsymbol{\Phi}_1^{\mathrm{T}}$	$\mathbf{P}^{i\mathrm{T}}$
$\mathbf{P}$	$\mathbf{0}$	$\mathbf{L}_{\mathrm{I}}$	$\mathbf{0}$
$\boldsymbol{\Phi}_1$	$-\beta\left(\tilde{\lambda}_1^2\right)^R\mathbf{L}_{\mathrm{I}}$	$\left(\tilde{\lambda}_1^2\right)^R\mathbf{L}_{\mathrm{I}}$	$\beta\left(\tilde{\lambda}_1^2\right)^R\mathbf{L}_{\mathrm{I}}$
$\mathbf{P}^i$	$\mathbf{0}$	$\mathbf{0}$	$\mathbf{D}_{\mathrm{I}}$

Appendix B. The basic relations for Alt.2

Although, it is much simpler, the basic relations for Alt.2 are as follows

$$\mathbf{L}_{\mathrm{I}}\boldsymbol{\Phi}_1 + \bar{c}\,\mathbf{L}_{\mathrm{I}}\left(\dot{\mathbf{P}} - \dot{\mathbf{P}}^i\right) + \mathbf{R}_{\mathrm{I}}^e = \mathbf{0} \tag{B.1}$$

$$\begin{gathered}-2\beta\left(\tilde{\lambda}_1^2\right)^R\mathbf{L}_{\mathrm{I}}\left(\mathbf{P} - \mathbf{P}^i\right) - \tfrac{2\beta}{\bar{\omega}}\left(\tilde{\lambda}_1^2\right)^I\mathbf{L}_{\mathrm{I}}\left(\dot{\mathbf{P}} - \dot{\mathbf{P}}^i\right) + \left(\left(\tilde{\lambda}_1^2\right)^R + \beta^2\right)\mathbf{L}_{\mathrm{I}}\boldsymbol{\Phi}_1 \\ + \left(\tfrac{1}{\bar{\omega}}\left(\tilde{\lambda}_1^2\right)^I + 2\beta\bar{c}\right)\mathbf{L}_{\mathrm{I}}\dot{\boldsymbol{\Phi}}_1 + \bar{c}^2\mathbf{L}_{\mathrm{I}}\ddot{\boldsymbol{\Phi}}_1 = \mathbf{0}\end{gathered} \tag{B.2}$$

$$\bar{c}^2\,\mathbf{L}_{\mathrm{I}}\,\ddot{\mathbf{P}}^i + \mathbf{Q}_{\mathrm{I}}\,\dot{\mathbf{P}}^i + \mathbf{D}_{\mathrm{I}}\,\mathbf{P}^i = -\mathbf{E}_{\mathrm{I}}^i\,\mathbf{a}_g \tag{B.3}$$

Based on these relations, the explicit forms of generalized matrices ($\mathbf{M}_{\mathrm{I}}$, $\mathbf{C}_{\mathrm{I}}$ and $\mathbf{K}_{\mathrm{I}}$) are quite apparent:

Table B.1 Explicit form of generalized matrix $\mathbf{M}_{\mathrm{I}}$ (Alt.2)

	$\mathbf{P}^{\mathrm{T}}$	$\mathbf{\Phi}_1^{\mathrm{T}}$	$\mathbf{P}^{i\mathrm{T}}$
$\mathbf{P}$	$\mathbf{0}$	$\mathbf{0}$	$\mathbf{0}$
$\mathbf{\Phi}_1$	$\mathbf{0}$	$\bar{\mathrm{c}}^2\mathrm{L}_{\mathrm{I}}$	$\mathbf{0}$
$\mathbf{P}^i$	$\mathbf{0}$	$\mathbf{0}$	$\bar{\mathrm{c}}^2\mathrm{L}_{\mathrm{I}}$

Table B.2 Explicit form of generalized matrix $\mathbf{C}_{\mathrm{I}}$ (Alt.2)

	$\mathbf{P}^{\mathrm{T}}$	$\mathbf{\Phi}_1^{\mathrm{T}}$	$\mathbf{P}^{i\mathrm{T}}$
$\mathbf{P}$	$\bar{\mathrm{c}}\,\mathbf{L}_{\mathrm{I}}$	$\mathbf{0}$	$-\bar{\mathrm{c}}\,\mathbf{L}_{\mathrm{I}}$
$\mathbf{\Phi}_1$	$-\frac{2\beta}{\bar{\omega}}\left(\tilde{\lambda}_1^2\right)^I\mathbf{L}_{\mathrm{I}}$	$\left(\frac{1}{\bar{\omega}}\left(\tilde{\lambda}_1^2\right)^I + 2\beta\bar{c}\right)\mathbf{L}_{\mathrm{I}}$	$\frac{2\beta}{\bar{\omega}}\left(\tilde{\lambda}_1^2\right)^I\mathbf{L}_{\mathrm{I}}$
$\mathbf{P}^i$	$\mathbf{0}$	$\mathbf{0}$	$\mathbf{Q}_{\mathrm{I}}$

Table B.3 Explicit form of generalized matrix $\mathbf{K}_{\mathrm{I}}$ (Alt.2)

	$\mathbf{P}^{\mathrm{T}}$	$\mathbf{\Phi}_1^{\mathrm{T}}$	$\mathbf{P}^{i\mathrm{T}}$
$\mathbf{P}$	$\mathbf{0}$	$\mathbf{L}_{\mathrm{I}}$	$\mathbf{0}$
$\mathbf{\Phi}_1$	$-2\beta\left(\tilde{\lambda}_1^2\right)^R\mathbf{L}_{\mathrm{I}}$	$\left(\left(\tilde{\lambda}_1^2\right)^R + \beta^2\right)\mathbf{L}_{\mathrm{I}}$	$2\beta\left(\tilde{\lambda}_1^2\right)^R\mathbf{L}_{\mathrm{I}}$
$\mathbf{P}^i$	$\mathbf{0}$	$\mathbf{0}$	$\mathbf{D}_{\mathrm{I}}$